A Hierarchical Study of the Reactions of Hydrogen Atoms with Alkenes: A Theoretical Study of the Reactions of Hydrogen Atoms with $C_2 - C_4$ Alkenes

Jennifer Power[1], Kieran P. Somers[1], Shashank S. Nagaraja[1], Henry J. Curran*[1]

[1]Combustion Chemistry Centre, School of Chemistry, Ryan Institute, MaREI, National University of Ireland, Galway, Galway H91TK33, Ireland

Corresponding author: henry.curran@nuigalway.ie

Abstract

The present study complements our previous studies on the reactions of hydrogen atoms with C_5 alkene species including 1- and 2-pentene and the branched isomers (2-methyl-1-butene, 2-methyl-2-butene, and 3-methyl-1-butene), by studying the reactions of hydrogen atoms with $C_2 - C_4$ alkenes (ethylene, propene, 1- and 2-butene, and isobutene). The aim of the current work is to develop a hierarchical set of rate constants for Ḣ atom addition reactions to $C_2 - C_5$ alkenes, both linear and branched, which can be used in the development of chemical kinetic models. High-pressure limiting and pressure-dependent rate constants are calculated using Rice-Ramsperger-Kassel-Marcus (RRKM) theory and a one-dimensional master equation (ME). Rate constant recommendations for Ḣ atom addition and abstraction reactions in addition to alkyl radical decomposition reactions are also proposed and provide a useful tool for use in mechanisms of larger alkenes for which calculations do not exist. Additionally, validation of our theoretical results with single-pulse shock-tube pyrolysis experiments is carried out. An improvement in species mole fractions predictions for alkene pyrolysis is observed, showing the relevance of the present study.

SUBJECTS: Alkenes, Hydrogen atoms, Alkyl radicals, Single-pulse shock-tube, Pyrolysis

1. Introduction

Alkenes are important intermediates formed during the oxidation and pyrolysis of larger alkanes and are key components of hydrocarbon fuels. An understanding of their combustion chemistry is therefore important in our understanding of hydrocarbon fuel combustion. The reactions of Ḣ atom across the C=C double bond plays an important role in controlling

experimental high-temperature ignition delay times (IDTs), flame speeds and species profiles measured as a function of temperature and/or time in jet-stirred and flow reactors.[1-3]

In the current work, the reactions of Ḣ atoms with $C_2 - C_4$ alkenes are studied, while the reactions of Ḣ atom addition to C_5 alkenes were studied previously.[4-5] There have been a number of theoretical and experimental studies of Ḣ atoms with $C_2 - C_4$ alkenes.[6-19] This study aims to complement these by providing a comprehensive hierarchical set of rate constants for Ḣ atom addition and abstraction potential energy surfaces (PES's), including their chemically activated pathways for $C_2 - C_5$ alkenes, determined at the same levels of theory. By having a consistent set of rate constants for $C_2 - C_5$ alkenes + Ḣ atoms calculated at the same level of theory, our results help constrain available models and the development of recommended rate constants which provide a tool for use in mechanisms of larger alkenes for which calculations do not exist in the literature.

Ethylene is the smallest alkene in our series and has been extensively studied.[6, 10-19] Miller and Klippenstein[6] studied the kinetics of Ḣ + C_2H_2 and Ḣ + C_2H_4, including their reverse dissociation reactions using variational transition state theory (VTST) and a 2-D master equation. Matsugi[19] performed direct trajectory calculations on $\dot{C}_2H_5$ radical dissociation and discovered a reaction pathway that directly eliminates H_2 from $\dot{C}_2H_5$, leading to the formation of vinyl ($\dot{C}_2H_3$) radicals. The resulting $\dot{C}_2H_3$ radicals can dissociate to C_2H_2 + Ḣ. They suggest that this may be an explanation for the unexpectedly slow Ḣ atom formation previously observed in photo-dissociation experiments of $\dot{C}_2H_5$ radicals.[20-21] Barker et al.[10] studied the reaction of Ḣ + C_2H_4 as a function of He pressure at room temperature with three experimental techniques; (i) a discharge flow system with Lyman-α photometry, (ii) a time resolved Lyman-α photometric system and (iii) a discharge flow system with time-of-flight mass spectrometry. Rate constants were obtained in both excess ethylene and hydrogen environments and an experimental value for the third body recombination coefficient for Ḣ + $\dot{C}H_3$ (+M) was obtained.

Michael et al.[15] used Lyman-α photometry to obtain the pressure dependence of the Ḣ + C_2H_4 reaction at room temperature. Through computer simulation analysis, the rate constants were adjusted for Ḣ atom depletion in reactions subsequent to the initial reaction. Experiments at high pressures of He permitted extrapolation to the high-pressure limit of the rate constant. Lee et al.[13] experimentally measured the rate constant for the Ḣ + C_2H_4 reaction as a function of temperature (198 – 320 K) at high pressures of Ar bath gas using the flash photolysis-resonance fluorescence technique. Sugawara et al.[17] measured the high-pressure limiting rate

constants of Ḣ and Ḋ atom addition to C_2H_4, C_2H_3D, C_2D_4, C_2H_2 and C_2D_2 in the temperature range 206 – 461 K using pulse radiolysis-resonance absorption.

Pacey et al.[16] performed pyrolysis experiments on ethane at 902 K and concentrations of $1.8 \times 10^{-4} – 4.5 \times 10^{-3}$ mol L^{-1} in a flow system. Rate constants for the reactions $\dot{C}_2H_5 + \dot{C}_2H_5 \leftrightarrow C_4H_{10}$ and $\dot{C}_2H_5 + \dot{C}_2H_5 \leftrightarrow C_2H_6 + C_2H_4$ were determined. Moreover, pressure-dependent rate constants for $C_2H_6 \leftrightarrow \dot{C}H_3 + \dot{C}H_3$ and $\dot{C}_2H_5 \leftrightarrow C_2H_4 + \dot{H}$ were determined using unimolecular reaction rate theory. Lightfoot et al.[14] measured the rate constant of the reaction $\dot{H} + C_2H_4 \leftrightarrow \dot{C}_2H_5$ as a function of temperature and pressure, over the temperature and pressure ranges 285 – 604 K and 50 – 600 Torr respectively, using laser flash photolysis/resonance fluorescence, with helium diluent.

Feng et al.[11] investigated the unimolecular decomposition of $\dot{C}_2H_5$ radicals in helium over the temperature and pressure ranges 876 – 1094 K and 0.8 – 14.3 Torr, respectively in time-resolved experiments. The reaction was isolated for quantitative study in a heated tubular reactor coupled to a photoionization mass spectrometer. Hanning et al.[12] studied the reaction $\dot{H} + C_2H_4 \leftrightarrow \dot{C}_2H_5$ at 800 K in He. Exciplex laser flash photolysis at 193.3 nm of ethene-helium mixtures was used to generate Ḣ atoms, which were detected using time-resolved resonance fluorescence. Rate coefficients for the forward and reverse reactions were deduced from measurements of the equilibrium constant and relaxation rate coefficient at nine pressures in the range 97 – 600 Torr. More recently, Yang et al.[18] investigated the decomposition of ethyl iodide and subsequent dissociation of ethyl radicals behind incident shock waves in a diaphragm-less shock tube using laser schlieren (LS) densitometry ($1150 \leq T \leq 1870$ K, and $55 \leq p \leq 123 \pm 3$ Torr).

Fewer studies exist for the reactions of Ḣ atoms with propene and the butene isomers. Experimental studies of Ḣ atoms with propene include, [8, 22-31] with the most recent one by Chen et al.[8] studying the temperature and pressure dependence of the product branching ratio of the Ḣ + propene reaction. This was done behind reflected shock waves in a diaphragm-less shock-tube using the Ḣ-ARAS technique in the temperature range 1065 – 1306 K at 1 and 2 bar. Quantum chemistry calculations were also performed at the CCSD(T)/CBS//CCSD/6-311++G(3df,2p) level of theory. The predicted high-pressure limit rate constant ratio for terminal versus non-terminal addition agrees well with that reported by Manion et al.[9] for the analogous reaction of Ḣ atoms with butene. Both Chen et al.[8] and Manion et al.[9] state that their predicted branching ratio for terminal versus non-terminal addition differ to that calculated by Miller and Klippenstein who studied the dissociation of propyl radicals and other reactions on

the $\dot{C}_3H_7$ PES.[7] With minor adjustments to several of the barrier heights, Miller and Klippenstein showed excellent agreement between their theoretical values and experimental results available in the literature over a wide range of conditions.

Manion and Awan [9] investigated the kinetics of terminal and internal Ḣ atom addition to 1-alkenes. Single-pulse shock tube methods were employed to thermally generate Ḣ atoms and their reactions with 1-butene were investigated over the temperature and pressure ranges of 880 – 1120 K and 145 – 245 kPa, respectively. Relative and absolute rate constants for the displacement of methyl and ethyl radicals by Ḣ atoms were determined and related to the high-pressure limit rate constant for Ḣ atom addition to the terminal and internal sites of 1-butene. It was found that addition to the terminal site is favored by a factor of 2.6 ± 0.4 at 1000 K. These results were combined with data from lower temperatures and used by Manion and Awan to derive rate constants in the temperature range 220 – 2000 K. They state that these branching ratio expressions should approximate the behavior of other un-branched 1-olefins and can thus be used as estimates for unstudied 1-olefins in detailed kinetic models describing pyrolysis and combustion conditions. A factor of three discrepancy was noted in the branching ratio for terminal to internal Ḣ atom addition by comparing their current experimental results with the theoretical study,[7] and they suggest that the difference observed is well outside the experimental errors of their study and any expected differences for 1-butene.

Wang et al.[32] studied the reaction kinetics of H-atom abstraction from C_4–C_6 alkenes by Ḣ atoms and $\dot{C}H_3$ radicals using the G4 composite method with CTST and Eckart tunneling corrections. The study provides the first systematic study on the key initiation abstraction reaction classes for alkenes with Ḣ atoms and $\dot{C}H_3$ radicals. However, large discrepancies are observed between the Wang et al.[32] calculations and those already present in the literature and calculated in this work.

Nagaraja et al.[31] performed a single-pulse shock-tube study on the pyrolysis of 2% $C_2 - C_6$ 1-alkenes at 2 bar in the temperature range 900 – 1800 K, with reactant intermediate and product species obtained and quantified using gas chromatography-mass spectrometry analysis.

One of the aims of the present study is to investigate the ratio of terminal to internal Ḣ atom addition to $C_2 - C_5$ alkenes taking into account our past studies [4-5] of the C_5 alkenes since discrepancies remain in the literature. Rate constant recommendations for Ḣ atom addition, abstraction and alkyl radical decomposition reactions will also be made and should serve as a useful tool for their use in mechanisms for larger alkenes where calculations do not exist.

Section 2 describes the computational methods employed in the current work and Section 3 presents the theoretical results including comparisons with literature studies, where available. Section 4 presents our simulation results compared to the shock tube pyrolysis experiments of Nagaraja et al. [31, 33]

Table 1. Summary of Experimental and theoretical studies relevant to $C_2 - C_4$ alkenes + Ḣ.

Year	Author	Reaction(s)	*T* (K)	*p* (kPa)	Method
2020	Nagaraja et al. [31]	pyrolysis of C_2–C_6 1-alkenes	900–1800	200	single pulse shock tube (SPST)
2020	Chen et al. [8]	Ḣ + C_3H_6	1065–1306	100 – 200	Ḣ-ARAS / shock-tube CCSD(T)/CBS//CCSD/6-311++G(3df,2p)
2018	Wang et al. [32]	C_4–C_6 alkenes + Ḣ and $\dot{C}H_3$			G4 composite method
2015	Manion et al. [9]	Ḣ + C_4H_8-1	880–1120	145 – 245	single pulse shock tube (SPST)
2013	Matsugi et al. [19]	photodissociation of $\dot{C}_2H_5$	–	–	direct trajectory calculations ώB97X-D / 6-31 + G(d,p)
2013	Miller et al. [7]	dissociation of propyl radicals & other reactions on $\dot{C}_3H_7$ potential	–	0 – HPL	CCSD(T)/cc-pVTZ MP2/6-311++G(d,p)
2012	Yang et al. [18]	decomposition of ethyl iodide / dissociation of $\dot{C}_2H_5$ radicals	1150–1870	7.3 – 16.4	diaphragmless shock tube / laser schlieren (LS) densitometry
2011	Rosado-Reyes et al. [27]	Ḣ + C_3H_6	922–1200	150 – 340	single pulse shock tube (SPST)
2004	Miller et al. [6]	Ḣ + C_2H_2 and C_2H_4	300–2000	>0.13 / HPL	variational transition state theory (VTST), 2D master equation

1993	Hanning et al. [12]	$\dot{H} + C_2H_4$	800	12.9 – 80.0	exciplex laser flash photolysis / time-resolved resonance fluorescence
1993	Feng et al. [11]	Unimolecular decomposition of $\dot{C}_2H_5$	876–1094	0.1 – 1.9	heated tubular reactor / to a photoionization mass spectrometer
1993	Seakins et al. [22]	$i\dot{C}_3H_7$ decomposition	720–910	–	Laser flash photolysis / photoionisation mass spectrometry
1992	Tsang [34]	Database for hydrocarbon pyrolysis		–	Estimate
1992	Hidaka et al. [28]	Thermal decomposition of C_3H_6	1200–1800	–	Laser kinetic absorption spectroscopy / GC
1991	Tsang [35]	Database for hydrocarbon pyrolysis	–	–	Estimate
1989	Loser et al. [29]	$\dot{H}$ atom abstraction by allyl radicals from hydrocarbons	–	–	BSBL
1987	Lightfoot et al.[14]	$\dot{H} + C_2H_4$	285 – 604	6.7 – 80.0	laser flash photolysis / resonance fluorescence
1986	Munk et al. [24]	$i\dot{C}_3H_7$ and $i\dot{C}_3H_7O_2$	298	101	UV absorption / pulse photolysis
1984	Pacey et al. [16]	Pyrolysis of C_2H_6	902	HPL	flow system

1982	Watanabe et al. [26]	$\dot{H} + C_3H_6$	200 – 500	–	Pulse radiolysis resonance absorption
1982	Harris et al. [30]	$\dot{H} + C_3H_6 / C_4H_8$	298–455	–	Flash photolysis resonance fluorescence
1981	Sugawara et al. [17]	$\dot{H}$ and D-atom addition to C_2H_4, C_2H_3D, C_2D_4, C_2H_2 and C_2D_2	206–461	–	Pulse radiolysis-resonance absorption.
1978	Lee et al. [13]	$\dot{H} + C_2H_4$	198–320	0.13	flash photolysis-resonance fluorescence (FP-RF) technique
1973	Michael et al. [15]	$\dot{H} + C_2H_4$	–	–	Lyman α photometry
1972	Kerr et al. [23]	Evaluated kinetic data on gas phase addition reactions	–	–	
1971	Kurylo et al. [25]	$\dot{H} + C_3H_6$	298	–	Resonance fluorescence of Lyman α radiation
1970	Barker et al. [10]	$\dot{H} + C_2H_4$	–	–	Discharge Flow System with Lyman-α Photometry, Time resolved Lyman-α Photometric System and Discharge Flow System with Time-of-Flight Mass Spectrometry

2. Computational Details

2.1 Electronic structure calculations

As mentioned earlier, we have employed the same methods here as those used in our previous studies [4-5] to carry out all electronic structure calculations, thus the description here is brief. All calculations were carried out using Gaussian 09 [36] and Gaussian 16 [37] Conformational searches were performed, with the resulting lowest energy conformer optimised at the ωB97XD[38] / aug-cc-pVTZ[39] level of theory. An harmonic frequency analysis was simultaneously performed at the same level of theory to verify the nature of each stationary point.

Low-frequency torsional modes were treated via relaxed PES scans in 10-degree increments with the ωB97XD/6-311++G(d,p)[38] method, with the potential energies as a function of dihedral angle used as input for a one-dimensional (1-D) hindered rotor approximation as implemented in the Master Equation System Solver (MESS).[40]

To compute reaction barrier heights, single point energies for minima and transition states were calculated at the CCSD(T)/cc-pVXZ and MP2/cc-pVXZ (where X = D, T and Q) levels of theory. The resulting energies were extrapolated to the complete basis set (CBS) limit using the following formula (1). [41-42]

$$E_{CCSD(T)/CBS} = E_{CCSD(T)/cc\text{-}pVTZ} + (E_{CCSD(T)/cc\text{-}pVTZ} - E_{CCSD(T)/cc\text{-}pVDZ})\,(3^4 / 4^4 - 3^4) + E_{MP2/cc\text{-}PVQZ} + (E_{MP2/cc\text{-}pVQZ} - E_{MP2/cc\text{-}pVTZ})\,(4^4 / 5^4 - 4^4) - E_{MP2/cc\text{-}pVTZ} - (E_{MP2/cc\text{-}pVTZ} - E_{MP2/cc\text{-}pVDZ})\,(3^4 / 4^4 - 3^4).$$

The T_1 diagnostic for minima and transition state species is ≤ ~0.03, indicating that single reference methods to describe the wave function are appropriate.[41] However, for the $\dot{C}_2H_3$ radical well and the transition states of Ḣ atom addition to and abstraction from C_2H_4, the T_1 diagnostics are 0.04, 0.038 and 0.352, respectively. As a result, for the C_2 and C_3 reaction systems, ROCCSD(T)/aug-cc-pVXZ, (where X = T and Q) single point energies were also calculated since they were computationally achievable. The energies were extrapolated to the CBS limit using the formula (2):

$$E_{ROCCSD(T)/CBS} = E_{ROCCSD(T)/aug\text{-}cc\text{-}pVQZ} + (E_{ROCCSD(T)/aug\text{-}cc\text{-}pVQZ} - E_{ROCCSD(T)/aug\text{-}cc\text{-}pVTZ}) * 4^4/(5^4 - 4^4),$$

with the resulting T_1 diagnostics falling below 0.03. The largest difference in energy barriers as a result of using the two formulas was for H-atom abstraction from the primary vinylic sites of C_2H_4 and C_3H_6, where differences of 1.57 and 1.39 kJ mol^{-1} respectively, were observed.

These differences in energy barriers increased the rate constants for these reactions by a factor of 1.87 and 1.71 at 298 K.

2.2 Thermochemistry

The methods employed to calculate the thermochemical parameters of species are identical to those used in our previous studies,[4-5] with 0 K formation enthalpies determined via the isodesmic approach using the most recent ATcT values for the molecular and radical chaperones, and uncertainties computed using methods described by Simmie et al.[43] Temperature-dependent enthalpies, entropies, and heat capacities were calculated using traditional statistical thermodynamic methods as implemented in MESSPF,[40] with Chemkin format polynomials fitted using PAC99,[44] and are provided as Supplementary material (SM).

2.3 Transition-State Theory (TST), Rice-Ramsperger-Kassel-Marcus (RRKM), and Master Equation (ME) Calculations

High-pressure limiting and pressure-dependent rate constants were calculated for the C_2 – C_4 PESs using RRKM/ME as implemented in MESS,[40] in which tunnelling is accounted for via an asymmetric Eckart model.[45] To model collisional energy transfer, a single exponential down model was used and is estimated to be $\langle\Delta E_{down}(T)\rangle = 75 \times (T/300)^{1.05}$ cm^{-1} for the $\dot{C}_2H_5$ PES [6] and $\langle\Delta E_{down}(T)\rangle = 200 \times (T/300)^{0.75}$ cm^{-1} for the $\dot{C}_3H_7$ and $\dot{C}_4H_9$ PESs. [46-49]

3. Theoretical Results

3.1 Thermochemistry

Table 2 presents formation enthalpies, along with their 2σ uncertainties computed via isodesmic and atomisation methods. Also presented are ATcT,[50-51] ANL0,[52] and ANL1.[52] formation enthalpies with 2σ uncertainties. The current study uses the most recent ATcT values for the molecular and radical chaperones.[50-51] Similar to previous work, [4-5] ATcT, ANL0 and ANL1 formation enthalpies do not exist for the species $\dot{C}_4H_7$-11, $\dot{C}_4H_7$-12, $\dot{C}_4H_7$-13, $\dot{C}_4H_7$-14, $\dot{C}_4H_7$-22, i$\dot{C}_4H_7$, and i$\dot{C}_4H_7$-i1. Quantum chemical composite methods (CBS–QB3, CBS–APNO, G3, and G4)[53-55] were therefore used to calculate their formation enthalpies at 0 K via isodesmic reactions suitable for each species, using ATcT values as chaperones.

Table 2. Formation enthalpies and uncertainties (2σ) computed via isodesmic and atomisation methods, together with ATcT, ANL0, and ANL1 formation enthalpies and uncertainties.

Species	isodesmic (0 K, kJ mol^{-1})	isodesmic (2σ)	atomisation (0 K, kJ mol^{-1})	atomisation (2σ)	ATcT[50-51] (0 K, kJ mol^{-1})	ANL0[52]	ANL1[52]	Burcat[56] (0 K, kJ mol^{-1})
C_2H_4	60.60	0.45	61.36	3.85	60.88	60.20	60.20	61.03
$\dot{C}_2H_5$	131.65	0.74	131.06	6.65	131.06	131.30	131.00	130.77
$\dot{C}_2H_3$	301.49	0.96	301.26	5.41	301.13	300.90	300.50	300.87
C_3H_6	35.03	0.36	35.85	7.33	34.93	34.50	–	35.01
$n\dot{C}_3H_7$	117.78	0.66	118.15	9.75	118.34	118.20	–	119.15
$i\dot{C}_3H_7$	105.33	0.92	105.71	9.63	105.32	105.10	–	108.24
$\dot{C}_3H_5$-s	277.86	0.87	278.38	7.53	278.22	278.40	–	276.29
$\dot{C}_3H_5$-t	262.28	0.95	262.80	6.86	262.98	263.00	–	
$\dot{C}_3H_5$-a	177.44	2.00	179.03	6.69	180.03	179.60	–	180.40
C_4H_8-1	21.15	0.20	22.40	10.66	21.00	21.30	–	20.82
C_4H_8-2	9.40	0.25	10.63	10.86	9.38	9.60	–	9.39
$\dot{C}_4H_9$-1	102.20	0.77	102.52	13.08	102.74	103.20	–	105.91
$\dot{C}_4H_9$-2	90.76	0.74	91.55	12.82	90.84	90.90	–	94.95
$\dot{C}_4H_7$-11	263.61	0.79	263.97	10.27	–	–	–	262.76
$\dot{C}_4H_7$-12	248.88	0.81	249.16	9.84	–	–	–	248.45
$\dot{C}_4H_7$-13	152.70	0.81	152.04	9.48	–	–	–	153.55
$\dot{C}_4H_7$-14	222.83	0.77	224.34	12.26	–	–	–	220.92
$\dot{C}_4H_7$-22	239.46	1.24	240.21	9.97	–	–	–	239.74
iC_4H_8	3.61	0.31	5.19	10.72	4.01	4.20	–	3.46
$i\dot{C}_4H_9$	96.14	0.73	96.38	12.91	97.17	–	–	97.92
$t\dot{C}_4H_9$	73.86	0.73	75.31	13.23	75.60	–	–	79.72
$i\dot{C}_4H_7$	153.25	0.81	153.73	9.49	–	–	–	155.27
$i\dot{C}_4H_7$-i1	250.60	0.70	251.18	10.45	–	–	–	

Excellent agreement is observed between this work and the ATcT[50-51] values, with differences, expressed as mean absolute error (MAE ± 2σ), being on average 0.59 ± 1.38 kJ mol^{-1}. Differences between this work and ANL0[52] and ANL1[52] computations are on average 0.57 ± 1.03 and 0.68 ± 0.60 kJ mol^{-1}, respectively. Differences between this work and Burcat[56] are slightly higher at 1.58 ± 3.2 kJ mol^{-1}. Comparisons between isodesmic and atomisation values calculated in the current work are in excellent agreement, with a MAE of 0.76 ± 0.93 kJ mol^{-1}. As discussed in our previous work,[4-5] although the isodesmic and atomisation methods give similar nominal 0 K heats of formation, the isodesmic method is often used to achieve "chemical accuracy". Our computed final heat of formation uncertainties for the isodesmic reactions are between 0.36 and 2.00 kJ mol^{-1}.

Table 3. Comparisons of the formation enthalpies computed in this work with literature data.

Species	$\Delta_f H_{298K}$ (this work)	$\Delta_f H_{298K}$ (Goldsmith)[41]	$\Delta_f H_{298K}$ (ATcT)[50-51]	$\Delta_f H_{298K}$ (Burcat)[56]
C_2H_4	51.99	52.30	52.36	52.50
$\dot{C}_2H_5$	120.61	120.92	119.99	119.70
$\dot{C}_2H_3$	297.29	297.90	296.93	296.58
C_3H_6	19.88	19.25	19.93	20.00
$n\dot{C}_3H_7$	100.23	101.67	100.94	101.32
$i\dot{C}_3H_7$	87.92	88.70	88.45	90.19
$\dot{C}_3H_5$-s	267.07	268.19	267.38	265.53
$\dot{C}_3H_5$-t	251.79	253.13	252.58	237.65
$\dot{C}_3H_5$-a	165.55	169.87	168.31	168.60
C_4H_8-1	–0.21	–0.00	0.05	–0.03
C_4H_8-2	–11.30	–11.30	–11.18	–11.19
$\dot{C}_4H_9$-1	78.86	80.75	80.23	81.80
$\dot{C}_4H_9$-2	68.02	69.45	66.07	70.22
$\dot{C}_4H_7$-11	246.82	248.11	–	245.87
$\dot{C}_4H_7$-12	232.66	–	–	231.16
$\dot{C}_4H_7$-13	135.21	137.65	–	136.11
$\dot{C}_4H_7$-14	206.50	208.36	–	204.60
$\dot{C}_4H_7$-22	223.32	225.10	–	223.85
iC_4H_8	–17.60	–17.15	–17.05	–17.57
$i\dot{C}_4H_9$	72.29	74.48	73.18	73.79
$t\dot{C}_4H_9$	50.77	54.39	50.30	55.04
$i\dot{C}_4H_7$	134.68	139.32	–	137.60
$i\dot{C}_4H_7$-i1	233.84	–	–	–

Table 3 presents 298 K formation enthalpies between this work and literature data, with the results generally in good agreement. Differences between this work and Goldsmith[41] are on average 1.56 ± 2.61 kJ mol^{-1}. Excellent agreement is observed between this work and ATcT,

with a MAE of 0.76 ± 1.43 kJ mol^{-1}. The values reported by Burcat [56] are within 2.01 ± 5.90 kJ mol^{-1} of this work.

Table 4. Comparisons of entropies computed in this work with literature data.

Species	$S_{298\ K}$ (this work)	$S_{298\ K}$ (Goldsmith) [41]	$S_{298\ K}$ (Burcat) [56]
C_2H_4	218.66	218.82	219.32
$\dot{C}_2H_5$	247.38	247.27	242.98
$\dot{C}_2H_3$	233.38	233.47	233.66
C_3H_6	266.10	266.10	266.66
$n\dot{C}_3H_7$	289.91	289.95	290.46
$i\dot{C}_3H_7$	295.05	288.28	290.11
$\dot{C}_3H_5$-s	271.27	271.54	271.31
$\dot{C}_3H_5$-t	273.48	273.63	266.06
$\dot{C}_3H_5$-a	257.07	257.32	257.88
C_4H_8-1	307.77	306.27	305.37
C_4H_8-2	295.67	295.81	296.33
$\dot{C}_4H_9$-1	331.26	328.44	307.63
$\dot{C}_4H_9$-2	331.85	330.54	327.42
$\dot{C}_4H_7$-11	312.91	311.71	311.28
$\dot{C}_4H_7$-12	315.08	–	300.37
$\dot{C}_4H_7$-13	300.56	301.25	306.09
$\dot{C}_4H_7$-14	321.80	315.89	317.35
$\dot{C}_4H_7$-22	310.77	311.28	313.26
iC_4H_8	293.21	293.72	287.45
$i\dot{C}_4H_9$	319.07	319.66	304.66
$t\dot{C}_4H_9$	318.97	318.82	323.39
$i\dot{C}_4H_7$	293.08	293.72	300.80
$i\dot{C}_4H_7$-i1	305.54	–	–

Table 4 presents comparisons of entropies calculated in this work and the literature, with differences being larger than those observed for the enthalpies. Differences between Goldsmith[41] and this work are on average 1.13 ± 3.72 J K^{-1} mol^{-1}, while differences between those recommended by Burcat[56] and calculated here are on average 5.09 ± 11.64 J K^{-1} mol^{-1}. In the case of $i\dot{C}_3H_7$, the lowest energy conformer has Cs symmetry, with an assigned symmetry factor of one. If it is assumed that the symmetry factor of $i\dot{C}_3H_7$ is two, the entropy value drops from 295.05 to 289.29 J K^{-1} mol^{-1}, which is now only 1.01 J K^{-1} mol^{-1} larger than the value computed by Goldsmith and 0.82 J K^{-1} mol^{-1} lower than that by Burcat [56]. For the $\dot{C}_4H_7$-14 radical, our computed entropy is 5.91 and 4.45 J K^{-1} mol^{-1} larger than Goldsmith [41] and Burcat[56], respectively. However, Goldsmith[41] reports an uncertainty of 5.86 J K^{-1} mol^{-1} for their reported entropy for $\dot{C}_4H_7$-14, and our value falls within this range.

Table 5. Comparisons of heat capacities computed here with literature data.

		Cp						
Species	Study	300	400	500	600	800	1000	1500
C_2H_4	This work	42.04	51.22	60.64	69.19	82.07	92.25	108.54
	Goldsmith [41]	42.68	52.30	61.50	69.87	82.84	92.88	109.20
	Burcat [56]	43.05	52.64	62.27	70.93	83.89	94.09	109.58
$\dot{C}_2H_5$	This work	50.83	60.85	70.92	80.13	94.66	106.31	125.31
	Goldsmith [41]	51.46	61.92	71.96	80.75	95.40	107.11	125.94
	Burcat [56]	50.86	61.26	71.64	81.13	96.05	107.91	126.21
$\dot{C}_2H_3$	This work	43.02	50.42	57.32	63.28	72.12	79.19	90.65
	Goldsmith [41]	43.51	51.46	58.16	63.60	72.80	79.50	91.21
	Burcat [56]	42.20	49.42	56.30	62.33	71.37	78.58	89.98
C_3H_6	This work	62.80	77.74	92.34	105.50	125.94	141.81	166.99
	Goldsmith [41]	64.43	79.91	94.56	107.11	127.61	143.09	168.20
	Burcat [56]	64.71	80.19	95.03	108.28	128.79	144.61	168.44
$n\dot{C}_3H_7$	This work	71.53	88.04	103.86	117.96	139.72	156.80	184.17
	Goldsmith [41]	72.38	89.96	105.86	119.24	141.42	158.16	185.35
	Burcat [56]	71.61	88.44	104.39	118.52	140.27	157.27	183.71
$i\dot{C}_3H_7$	This work	67.68	83.16	99.11	113.83	136.88	154.91	183.44
	Goldsmith [41]	68.62	84.94	100.83	115.06	138.49	156.06	184.51
	Burcat [56]	65.81	81.67	97.76	112.60	136.04	154.33	182.33
$\dot{C}_3H_5$-s	This work	62.51	75.45	87.65	98.44	115.11	128.06	148.67
	Goldsmith [41]	64.02	77.40	89.54	99.58	116.32	129.29	149.37
	Burcat [56]	63.63	76.53	88.46	98.97	115.47	128.30	148.22
$\dot{C}_3H_5$-t	This work	61.98	74.30	86.40	97.33	114.35	127.61	148.57
	Goldsmith [41]	63.18	76.15	87.86	98.74	115.90	128.87	149.37
	Burcat [56]	61.94	76.98	90.79	102.80	121.04	134.95	155.57
$\dot{C}_3H_5$-a	This work	61.33	76.91	90.74	102.38	119.28	132.16	152.54
	Goldsmith [41]	62.34	78.24	92.05	102.93	120.08	133.05	153.13
	Burcat [56]	62.12	77.74	91.51	103.04	119.77	132.52	152.17
C_4H_8-1	This work	84.31	105.66	125.90	143.81	171.31	192.50	225.95
	Goldsmith [41]	87.03	109.20	129.29	146.44	173.64	194.56	227.61
	Burcat [56]	85.96	106.28	126.08	144.16	173.16	195.04	227.47
C_4H_8-2	This work	85.63	105.06	124.29	141.89	169.82	191.32	225.43
	Goldsmith[41]	88.28	108.78	127.61	144.77	172.38	193.30	226.77
	Burcat[56]	88.03	108.22	127.84	145.62	173.80	195.38	227.77
$\dot{C}_4H_9$-1	This work	93.56	116.39	137.92	156.88	185.81	208.19	243.65
	Goldsmith [41]	96.23	119.24	140.58	158.57	187.86	210.04	245.18
	Burcat [56]	94.98	118.67	140.97	160.63	190.76	213.94	249.44
$\dot{C}_4H_9$-2	This work	90.04	111.14	132.42	151.82	181.88	205.36	242.30
	Goldsmith [41]	91.63	113.80	135.14	153.97	184.10	207.53	243.93
	Burcat [56]	86.79	109.43	131.47	151.27	181.88	205.47	241.32
$\dot{C}_4H_7$-11	This work	84.17	103.50	121.34	136.89	160.62	178.88	207.72
	Goldsmith [41]	86.19	106.27	123.85	138.91	162.34	180.33	208.78
	Burcat [56]	84.05	103.05	120.71	136.20	160.05	178.45	206.63

$\dot{C}_4H_7$-12	This work	83.70	102.27	120.04	135.77	159.75	178.27	207.41
	Goldsmith [41]							
	Burcat [56]	84.33	103.88	121.97	137.87	162.53	181.46	210.28
$\dot{C}_4H_7$-13	This work	81.56	101.65	120.62	137.24	162.13	181.10	210.74
	Goldsmith [41]	83.26	103.76	122.59	138.49	163.59	182.42	211.71
	Burcat [56]	81.15	101.15	120.07	136.69	161.70	180.78	209.69
$\dot{C}_4H_7$-14	This work	83.27	102.21	120.16	135.94	159.76	178.10	207.05
	Goldsmith [41]	86.61	105.86	123.43	138.49	161.92	179.91	208.36
	Burcat [56]	85.14	104.57	122.89	138.96	163.17	181.76	210.14
$\dot{C}_4H_7$-22	This work	83.12	99.93	116.93	132.58	157.36	176.52	206.64
	Goldsmith [41]	84.94	102.81	119.24	134.31	158.41	178.24	207.94
	Burcat [56]	83.51	99.85	116.58	132.13	157.01	176.30	205.65
iC_4H_8	This work	86.01	106.46	125.84	143.20	170.72	191.87	225.62
	Goldsmith [41]	88.28	109.20	128.87	145.60	172.80	193.72	227.19
	Burcat [56]	86.44	109.53	130.81	149.22	176.71	197.59	228.66
$i\dot{C}_4H_9$	This work	95.21	118.37	139.73	158.34	186.70	208.68	243.73
	Goldsmith [41]	96.65	120.92	142.26	160.25	188.70	210.46	245.18
	Burcat [56]	98.56	122.36	143.90	162.52	191.01	212.96	246.99
$t\dot{C}_4H_9$	This work	88.45	108.45	129.49	149.13	180.04	204.10	241.76
	Goldsmith [41]	90.79	111.29	132.21	151.04	182.00	205.85	243.09
	Burcat [56]	82.78	104.42	126.31	146.47	178.31	202.90	240.05
$i\dot{C}_4H_7$	This work	80.50	102.35	121.72	138.17	162.72	181.35	210.69
	Goldsmith [41]	82.01	104.18	123.43	139.33	164.01	182.42	211.71
	Burcat [56]	82.59	103.51	122.32	138.44	162.74	181.30	209.76
$i\dot{C}_4H_7$-i1	This work	85.77	103.91	120.75	135.71	159.46	177.78	207.03
	Goldsmith [41]	–	–	–	–	–	–	–
	Burcat [56]	–	–	–	–	–	–	–

Table 5 presents heat capacities for the $C_2 – C_4$ species calculated in this work, by Goldsmith[41] and present in the Burcat database.[56] Good agreement is observed, with a MAE of 1.69 ± 1.5 J mol^{-1} K^{-1} observed between this work and Goldsmith.[41] Differences between this work and the Burcat database[56] are slightly higher, with a MAE of 1.87 ± 3.36 J K^{-1} mol^{-1}.

3.2 Reactions of Ḣ atoms with C_2H_4, C_3H_6, C_4H_8-1, C_4H_8-2, and iC_4H_8

Table 6. Computed energy barriers, heats of reaction, and high-pressure limiting rate constant (298 – 2000 K) for the reactions of Ḣ atoms with C_2 – C_4 alkenes. Units (AT^n = cm^3 mol^{-1} s^{-1}, energies kJ mol^{-1}).

		Reaction	$\Delta^{\ddagger}H_{0K}$	$\Delta_r H_{0K}$	A	n	E_a
C_2	R1	$C_2H_4 + \dot{H} \leftrightarrow \dot{C}_2H_5$	11.18	–146.48	1.15×10^{15}	–0.41	14.73
	R2	$C_2H_4 + \dot{H} \leftrightarrow \dot{C}_2H_3 + H_2$	63.12	24.09	4.79×10^{05}	2.55	51.77
C_3	R3	$C_3H_6 + \dot{H} \leftrightarrow n\dot{C}_3H_7$	15.61	–132.97	6.25×10^{15}	–0.73	19.34
	R4	$C_3H_6 + \dot{H} \leftrightarrow i\dot{C}_3H_7$	8.39	–146.83	1.02×10^{14}	–0.03	11.43
	R5	$C_3H_6 + \dot{H} \leftrightarrow \dot{C}_3H_5$-s $+ H_2$	63.97	27.14	1.21×10^{06}	2.43	53.96
	R6	$C_3H_6 + \dot{H} \leftrightarrow \dot{C}_3H_5$-t $+ H_2$	51.95	12.04	3.11×10^{05}	2.51	40.36
	R7	$C_3H_6 + \dot{H} \leftrightarrow \dot{C}_3H_5$-a $+ H_2$	31.09	–71.88	6.97×10^{02}	3.24	13.93
C_4	R8	C_4H_8-1 $+ \dot{H} \leftrightarrow \dot{C}_4H_9$-1	16.04	–136.49	2.23×10^{14}	–0.27	18.47
	R9	C_4H_8-1 $+ \dot{H} \leftrightarrow \dot{C}_4H_9$-2	9.32	–147.65	6.06×10^{15}	–0.60	14.59
	R10	C_4H_8-2 $+ \dot{H} \leftrightarrow \dot{C}_4H_9$-2	12.52	–136.08	1.56×10^{15}	–0.42	15.68
	R11	C_4H_8-1 $+ \dot{H} \leftrightarrow \dot{C}_4H_7$-11 $+ H_2$	64.81	27.38	2.01×10^{06}	2.44	54.53
	R12	C_4H_8-1 $+ \dot{H} \leftrightarrow \dot{C}_4H_7$-12 $+ H_2$	52.29	13.06	2.11×10^{05}	2.54	40.67
	R13	C_4H_8-1 $+ \dot{H} \leftrightarrow \dot{C}_4H_7$-13 $+ H_2$	22.85	–82.85	2.37×10^{05}	2.56	12.24
	R14	C_4H_8-1 $+ \dot{H} \leftrightarrow \dot{C}_4H_7$-14 $+ H_2$	42.70	–14.76	1.23×10^{05}	2.71	29.03
	R15	C_4H_8-2 $+ \dot{H} \leftrightarrow \dot{C}_4H_7$-13 $+ H_2$	33.51	–69.77	2.60×10^{04}	2.95	15.36
	R16	C_4H_8-2 $+ \dot{H} \leftrightarrow \dot{C}_4H_7$-22 $+ H_2$	54.25	15.91	1.21×10^{04}	2.41	43.19
	R17	$iC_4H_8 + \dot{H} \leftrightarrow i\dot{C}_4H_9$	21.15	–124.43	9.67×10^{13}	–0.21	22.08
	R18	$iC_4H_8 + \dot{H} \leftrightarrow t\dot{C}_4H_9$	6.13	–145.60	7.89×10^{15}	–0.53	11.98
	R19	$iC_4H_8 + \dot{H} \leftrightarrow i\dot{C}_4H_7 + H_2$	30.50	–63.73	4.45×10^{03}	3.08	14.81
	R20	$iC_4H_8 + \dot{H} \leftrightarrow i\dot{C}_4H_7$-i1 $+ H_2$	66.75	32.19	2.60×10^{06}	2.34	57.34

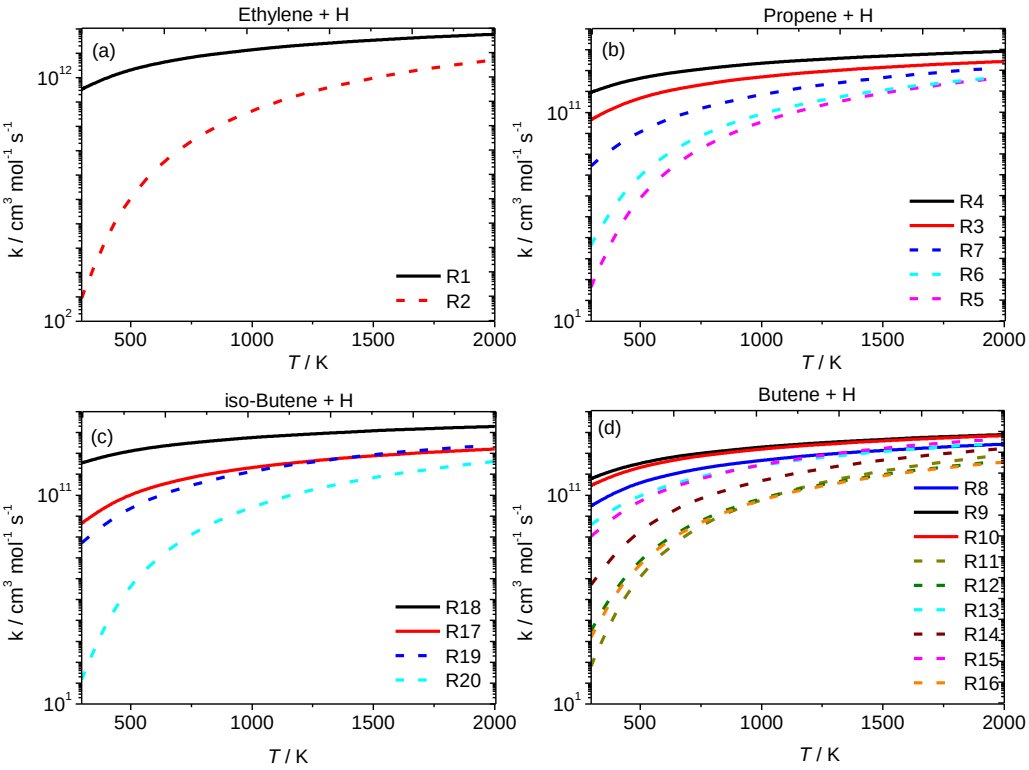

Figure 1. High pressure limit rate constants for the reactions of (a) ethylene + Ḣ, (b) propene + Ḣ, (c) isobutene + Ḣ, and (d) 1- and 2-butene + Ḣ.

Figure 1 compares the high-pressure limiting rate constants (Table 6), for (a) ethylene + Ḣ, (b) propene + Ḣ, (c) isobutene + Ḣ, and (d) 1- and 2-butene + Ḣ. Hydrogen atom addition to, and abstraction from, ethylene have computed energy barriers of 11.2 and 63.1 kJ mol^{-1}, respectively. Terminal Ḣ atom addition to propene has a computed energy barrier of 8.4 kJ mol^{-1}, which is 7.2 kJ mol^{-1} lower than that for internal addition. As expected, Ḣ atom abstraction from the primary allylic site of propene is favored, with an energy barrier of 31.1 kJ mol^{-1}. Abstraction of the two Ḣ atoms on the primary vinylic site have similar barriers of 63.7 and 64.6 kJ mol^{-1}, leading to cis- and trans- configurations of $\dot{C}_3H_5$-s, respectively. Terminal Ḣ atom addition to isobutene forming the tertiary t$\dot{C}_4H_9$ radical has a computed barrier of 6.1 kJ mol^{-1}, which is 15.0 kJ mol^{-1} lower than internal addition forming the primary i$\dot{C}_4H_9$ radical. Abstraction from the primary allylic site has a computed barrier of 30.5 kJ mol^{-1}. Terminal and internal Ḣ atom addition can exist for 1-butene, with respective barriers of 9.3 and 16.0 kJ mol^{-1}, while abstraction from the primary allylic site has a barrier of 22.85 kJ mol^{-1}. Internal addition to 2-butene and abstraction from the primary allylic site have respective barriers of 12.5 and 33.5 kJ mol^{-1}.

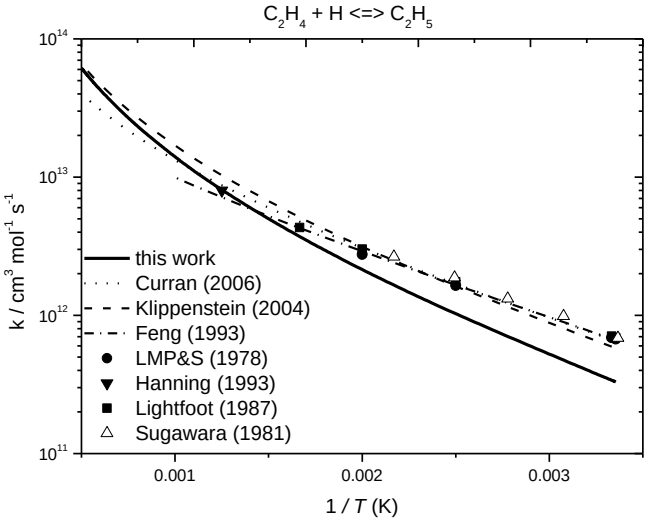

Figure 2. High-pressure limiting rate constant comparisons for the reactions of Ḣ atom addition with ethylene. Solid lines represent the current work (ROCCSD(T)/aug-cc-pVXZ), dotted (Curran[57]), dashed (Miller and Klippenstein[6]), dashed-dotted (Feng et al.[11]), ● (Lee et al.[13]), ▲ (Hanning et al.[12]), ■ (Lightfoot et al.[14]), and △ (Sugawara et al.[17]).

Figure 2. compares theoretical and experimental data [12-14, 17] for the reaction $C_2H_4 + \dot{H} \leftrightarrow \dot{C}_2H_5$. Also plotted is the rate constant recommendation from Curran et al. [57] and the transition state theory fit to the experiments by Feng et al.,[11] with good agreement being observed. The largest difference observed between the current work and Miller and Klippenstein [6] is a factor of 1.75 at 300 K. The difference in energy barrier of 0.54 kJ mol^{-1} and the quoted uncertainty of their fits to replicate the master equation results of ± 20%, which would account for an accumulative difference of ~1.5.

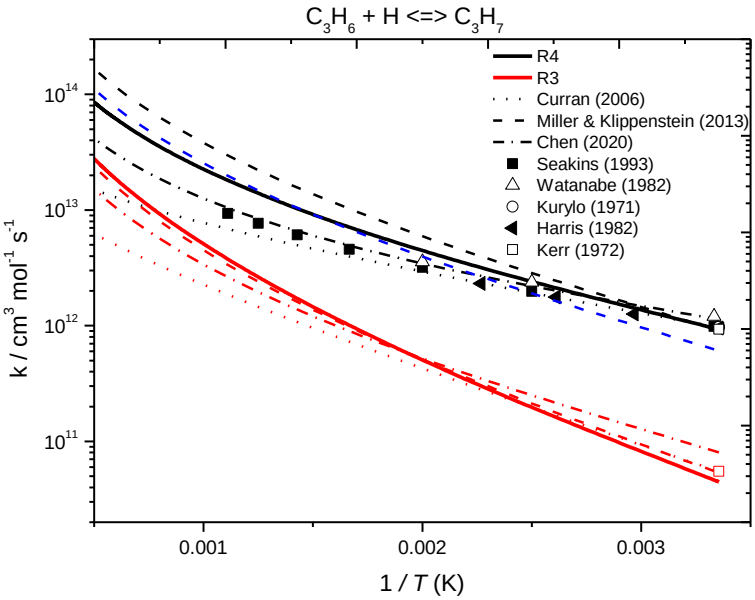

Figure 3. High-pressure limiting rate constant comparisons for the reactions of Ḣ atom addition to propene. Solid lines represent the current work (ROCCSD(T)/aug-cc-pVXZ), dotted (Curran[57]), dashed (Miller and Klippenstein[7]), dashed-dotted (Chen[8]), ■ (Seakins et al.[22]), △ (Watanabe et al.[26]), ○ (Kurylo et al.[25]), ◀ (Harris et al.[30]), and □ (Kerr et al.[23]).

Figure 3 presents high-pressure limiting rate constant comparisons for the Ḣ atom addition reactions to propene. Relatively good agreement is observed between the current work and theory and experiments from the literature. In order to improve agreement with experiment, Miller and Klippenstein[7] altered some reaction barriers, including those for terminal and internal H-atom addition and H-atom abstraction from the primary allylic site of propene. The adjusted rate constant for internal addition to propene (red) is in excellent agreement with the one calculated in the current work and the adjusted energy barrier of 15.5 kJ mol^{-1} is almost identical to 15.6 kJ mol^{-1} calculated in the current work, as shown in Table 6. The rate constant for terminal addition (black) is approximately a factor of two faster than that calculated here. However, as mentioned by Chen et al.,[8] the higher values reported by Miller and Klippenstein may be attributed to input data errors. An error in symmetry number affects the energy barriers and pressure dependent rate constant expressions. If the effect of symmetry reduced the rate constant by a factor of ~1.5 (dashed blue line, Fig 3), it would be in good agreement with that calculated here.

The rate constants reported by Chen et al.[8] are within a factor of two of the current work over the temperature range 298 – 2000 K. Differences in energy barriers computed in this work and that by Chen are 3.01 and 2.49 kJ mol^{-1} for non-terminal addition and terminal addition,

respectively. The recommendations by Curran et al.[57] are in good agreement at $T < 800$ K, but differences become larger at higher temperatures, with a factor of ~5 discrepancy observed at 2000 K.

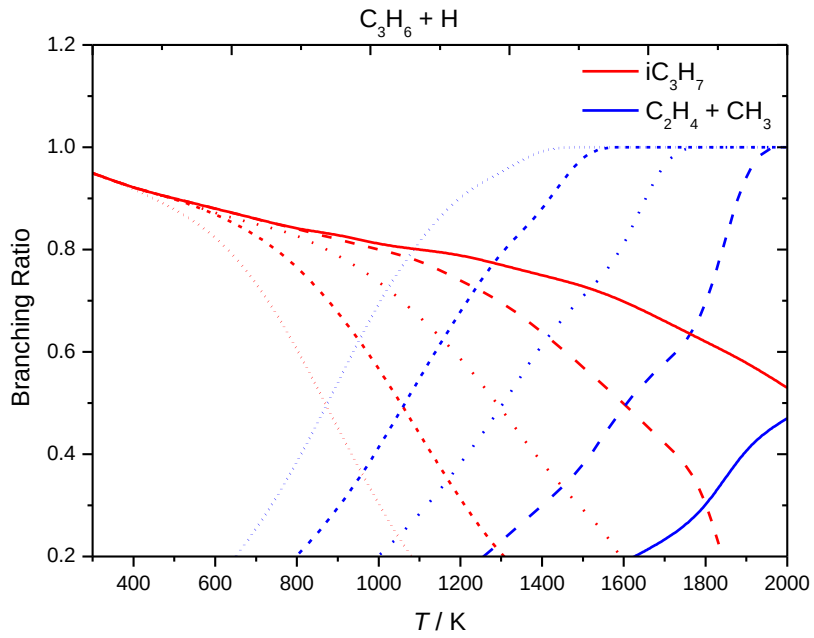

Figure 4. Temperature- and pressure-dependent branching ratios for propene + Ḣ via hydrogen atom addition reactions at 0.1 (short-dotted lines), 1 (short-dashed lines), 10 (dotted lines), 100 (dashed lines), and 1000 (solid lines) atm.

Figure 4 presents the temperature- and pressure-dependencies of the product branching ratios for Ḣ atom addition to propene in the temperature range 298 – 2000 K and at pressures of 0.1, 1.0, 10, 100 and 1000 atm. At 0.1 atm Ḣ atom addition to propene forming i$\dot{C}_3H_7$ radicals is favoured at temperatures up to 800 K, until the formation of C_2H_4 and $\dot{C}H_3$ dominates. For pressures of 1.0, 10, and 100 atm, the formation of i$\dot{C}_3H_7$ is favoured at temperatures up to ~1000 K, 1200 K, 1500 K respectively.

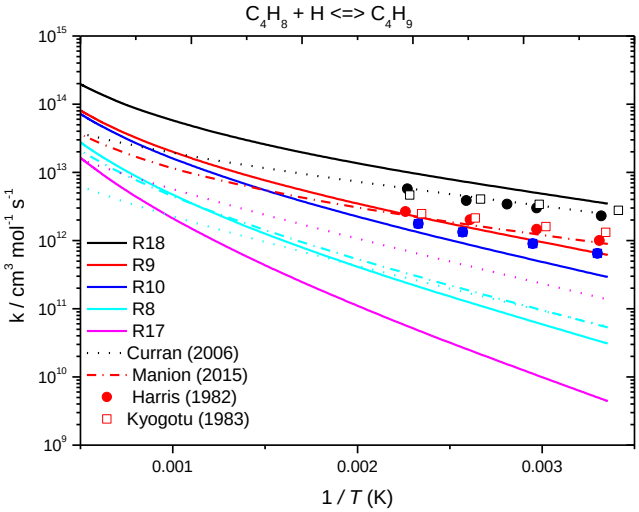

Figure 5. High-pressure limiting rate constant comparisons for the reactions of Ḣ atom addition to the butene isomers. Solid lines represent the current work (ROCCSD(T)/aug-cc-pVXZ) dotted (Curran[57]), dash-dotted (Manion et al.[9]), ● (Harris et al.[30]), and □ (Kyogotu et al.[58]).

Figure 5 presents high-pressure limiting rate constant comparisons for the reactions of Ḣ atom addition to the butene isomers. Larger differences are observed for the reactions of Ḣ atoms with C_4 alkenes calculated here and in the literature. For terminal addition to 1-butene, the rate constants determined by Manion et al.[9] and in this work are within a factor of ~2.22 over the temperature range 298 – 2000 K. The rate constants for internal addition to 1-butene are in excellent agreement and are within a factor of ~1.3. Additionally, the current calculations are in relatively good agreement with the experimental data by Kyogutu et al.[58] and Harris et al.[30] For terminal addition to isobutene, the recommendations by Curran et al.[57] are again in good agreement at lower temperatures but there is a larger deviation of a factor of five observed at 2000 K. The largest difference is observed for internal addition to isobutene. However, the difference in rate constants calculated in the current work for internal addition to 1-butene and isobutene is consistent with the difference in the computed barrier heights of 5.1 kJ mol^{-1}, accounting for the factor of seven discrepancy at low temperatures. Curran's recommendation is a factor of ~30 times faster at 298 K. The rate constant recommendation used is 2.5 times the recommendation used for internal addition to propene. However, it was found that our calculations for internal addition to propene is ~10 times faster than that to isobutene at 298 K, which can be attributed to the energy barrier for internal addition to propene being ~5.54 kJ mol^{-1} lower than that for isobutene.

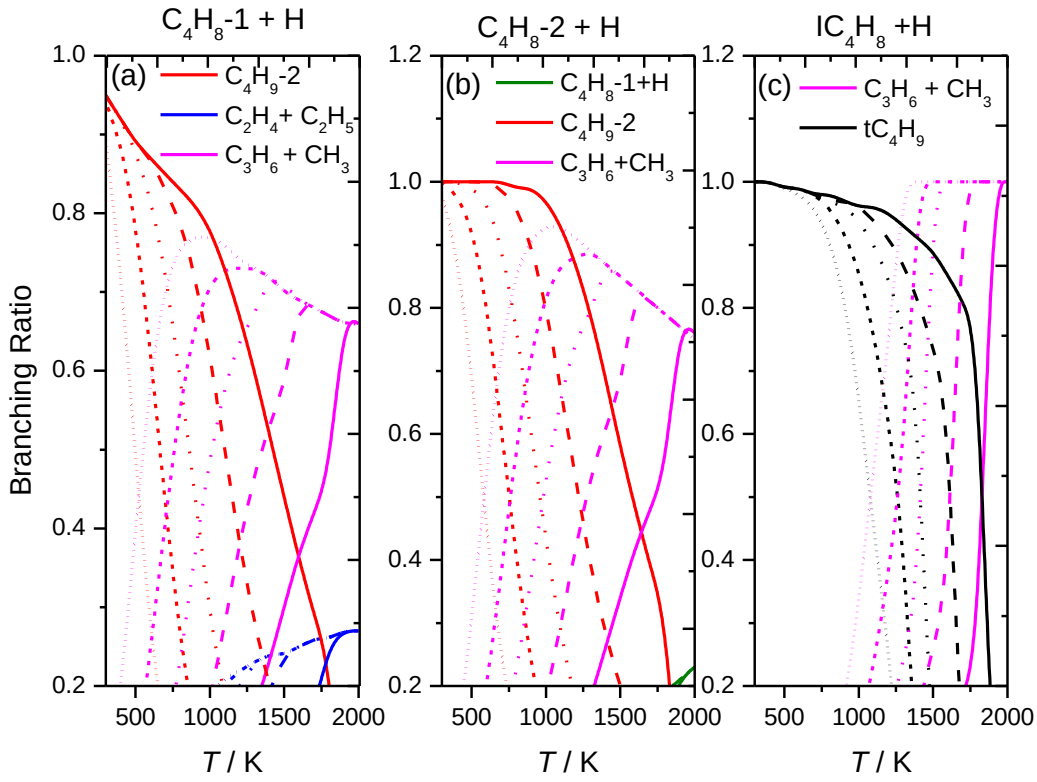

Figure 6. Temperature- and pressure-dependent branching ratios for (a) 1-butene, (b) 2-butene and (c) isobutene via hydrogen atom addition reactions at 0.1 (short-dotted lines), 1 (short-dashed lines), 10 (dotted lines), 100 (dashed lines), and 1000 (solid lines) atm.

Figure 6 shows the temperature- and pressure-dependencies of the product branching ratios for Ḣ atom addition to (a) 1- and (b) 2-butene and (c) isobutene in the temperature range 298 – 2000 K and at pressures of 0.1, 1.0, 10, 100 and 1000 atm. For both 1- and 2-butene, at 0.1 atm, Ḣ atom addition forming the $\dot{C}_4H_9$-2 radical is favoured at temperatures up to 500 K. The formation of C_3H_6 and $\dot{C}H_3$ then dominates the reaction flux at higher temperatures. Similar trends are observed in both Figs. 6(a) and (b) at 1.0, 10, and 100 atm. However the formation of $\dot{C}_4H_9$-2 is favoured at temperatures up to ~700, 900, and 1200 K, respectively. In the case of isobutene, Ḣ atom addition forming $t\dot{C}_4H_9$ radicals is favoured at temperatures up to 1000 K at 0.1 atm, whereas at higher temperatures the formation of C_3H_6 and $\dot{C}H_3$ dominates. The same trends are observed at 1.0, 10, and 100 atm. However the formation of $t\dot{C}_4H_9$ radicals is favoured at temperatures up to 1200, 1400, and 1600 K, respectively.

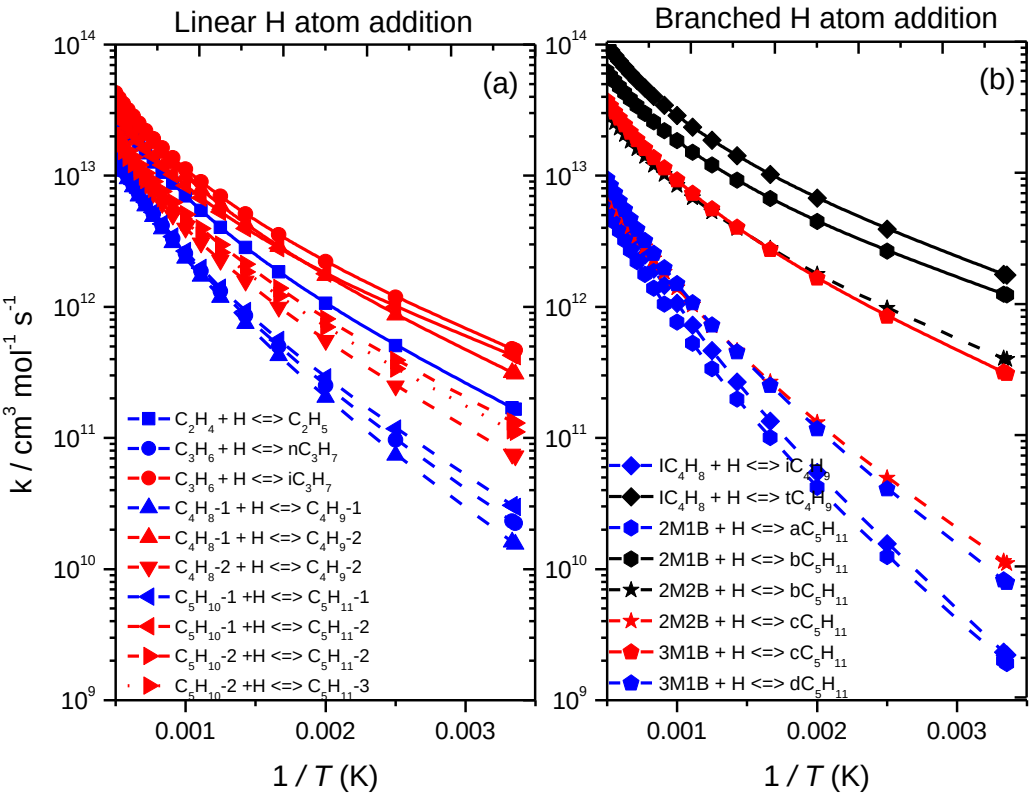

Figure 7. Rate constants (symmetry uncorrected) for terminal and internal Ḣ atom addition to (a) linear and (b) branched $C_2 - C_5$ alkenes from previous [4-5] and current work. Solid and dashed lines represent terminal and internal addition, respectively. Different colours represent different radical types formed. Black (tertiary), red (secondary) and blue (primary). Different symbols correspond to the different reactants. ■ (ethylene), ● (propene), ▲ (1-butene), ▼ (2-butene), ◆ (isobutene), ◀ (1-pentene), ▶ (2-pentene), ⬢ (2-methyl-1-butene), ★ (2-methyl-2-butene), and ⬟ (3-methyl-1-butene).

Figure 7 presents rate constants for Ḣ atom addition reactions, which are reported with no symmetry or optical isomer corrections between the transition state and reactants – i.e. the reaction path degeneracy is set to one. Table S1 of SM presents the symmetry factors for the reactants and transition states prior to this change. As expected, external Ḣ atom addition to each of the alkenes (solid lines) dominates over internal addition (dashed lines). For the linear alkenes, both external and internal Ḣ atom addition can lead to the formation of primary (blue) or secondary radicals (red). The rate constants for external addition to propene, 1-butene and 1-pentene are similar with respective barrier heights of 8.4, 9.3 and 7.8 kJ mol^{-1}. However, the rate constant for external addition to ethylene is approximately a factor of two slower than

external addition to propene and 1-butene at 500 K, reducing to a factor of ~1.4 at 2000 K. This difference can be attributed to the difference in energy barrier of ~2.8 kJ mol^{-1}. This can also be correlated with radical stability as a primary radical is formed in the case of ethylene, while secondary radicals are formed for propene, 1-butene and 1-pentene.

Internal Ḣ atom addition to linear alkenes form either primary ($C_3H_6 + \dot{H} \leftrightarrow n\dot{C}_3H_7$, C_4H_8-1 + Ḣ ↔ $\dot{C}_4H_9$-1, and C_5H_{10}-1 + Ḣ ↔ $\dot{C}_5H_{11}$-1) or secondary radicals (C_4H_8-2 + Ḣ ↔ $\dot{C}_4H_9$-2, C_5H_{10}-2 + Ḣ ↔ $\dot{C}_5H_{11}$-2, and C_5H_{10}-2 + Ḣ ↔ $\dot{C}_5H_{11}$-3). Rate constants for internal addition to propene, 1-butene and 1-pentene are similar. Rate constants for internal addition to 2-pentene are almost identical, with internal addition to 2-butene being slightly slower. However, this can be attributed to an energy barrier difference of ~1.6 kJ mol^{-1}.The branched alkenes have been described previously,[5] so we shall not re-iterate here. A trend was observed in that the rate constants for formation of tertiary radicals are the fastest, followed by secondary and primary radicals, respectively.[5] In the rate rule determinations, two rules were proposed for internal Ḣ-atom addition to branched alkenes (one for addition to a branched alkene where the branching occurs at the double bond and a second for where the branching does not occur at the double bond. For the cases where branching occurs at the double bond ($iC_4H_8 + \dot{H} \leftrightarrow i\dot{C}_4H_9$ and 2M1B + Ḣ ↔ $a\dot{C}_5H_{11}$), the energy barriers are similar, being 21.15 and 19.9 kJ mol^{-1}, and are higher than that for 3M1B + Ḣ ↔ $d\dot{C}_5H_{11}$ (17.15 kJ mol^{-1}), where the branching does not occur at the double bond.

Recommended rate constants were suggested based on (i) whether addition is to a linear or branched alkene (ii) whether it is terminal or internal addition and (iii) the type of radical formed. An average of the rate constants within each sub-class was taken as the recommended rate constant. If only one rate constant was available, for example in the case of internal addition to a branched alkene forming a secondary radical ($bC_5H_{10} + \dot{H} \leftrightarrow c\dot{C}_5H_{11}$), the rate constant for the reaction is taken as the recommended rate constant. For the rate constant recommendations presented in Tables 7, 9 and 11, the activation energies are expressed in cal mol^{-1} units for ease in implementing into kinetic mechanisms.

In relation to the uncertainty bounds presented in Tables 7, 9, and 11, upper and lower bounds are given, which are defined as:

$$\text{Upper} = k_{max} / k_{recommendation}$$

$$\text{Lower} = k_{recommendation} / k_{min}$$

where $k_{recommendation}$ refers to the recommended rate coefficient and k_{min} and k_{max} refer to the minimum and maximum rate coefficients used in the determinations of the recommended rate

coefficients, respectively. Appropriate symmetry corrections must be applied (Table 8) to these recommendations for use in rate rule determinations (Table 9).

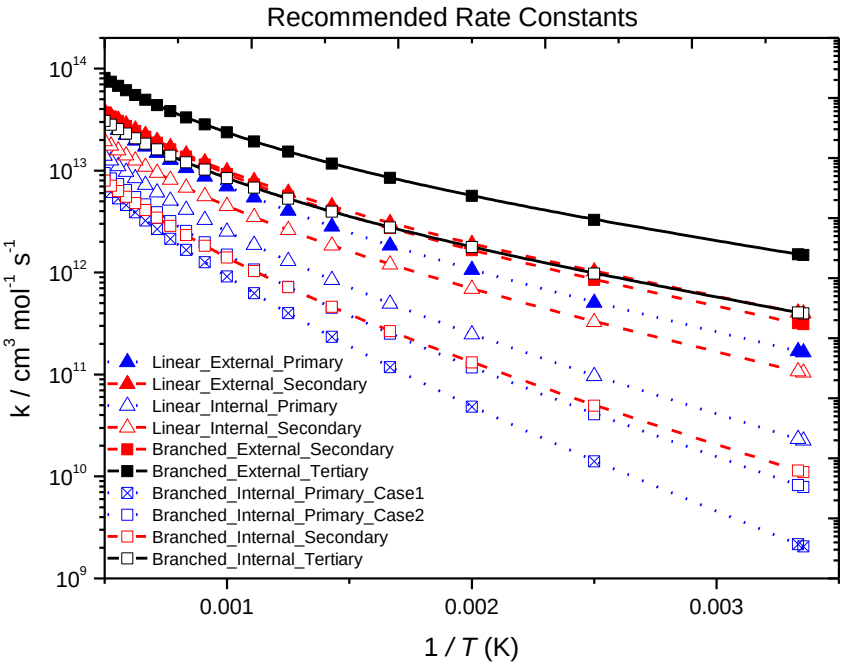

Figure 8. Rate constant recommendations (symmetry uncorrected) for Ḣ atom addition to linear (▲) and branched (■) C_2-C_5 alkenes. Solid, dashed and dotted lines represent the formation of tertiary, secondary and primary radicals, respectively. Open symbols are internal C-atom additions, solid symbols are external C-atom additions.

Table 7: Rate constant recommendations (symmetry uncorrected) for Ḣ atom addition to linear and branched alkenes (C_2-C_5).

Structure	**Site**	**Radical Formed**	***A***	***n***	***Ea***	**Uncertainty Bounds (Upper, Lower)**
Linear	External	1°	2.40×10^{08}	1.60	1526.	–
	External	2°	4.35×10^{08}	1.54	1144.	1.17, 1.23
	Internal	1°	7.79×10^{07}	1.67	2276.	1.32, 1.45
	Internal	2°	2.74×10^{08}	1.52	1621.	1.24, 1.43
Branched	External	2°	4.21×10^{08}	1.54	1292.	–
	External	3°	1.42×10^{09}	1.47	836.	1.22,1.29
	Internal_Case1	1°	2.27×10^{07}	1.78	3326.	1.18, 1.21
	Interna_Case2	1°	4.29×10^{07}	1.71	2677.	–

	Internal	2°	5.09×10^{07}	1.65	2401.	–
	Internal	3°	5.45×10^{08}	1.47	1070.	–

Table 8: Symmetry Corrections to be applied to rate constant recommendations for Ḣ-atom addition to alkenes.

σ Reactant	σ Transition State	Symmetry Corrected / Symmetry Uncorrected
1	0.5	2
2	0.5	4
2	1.0	2
4	2.0	2

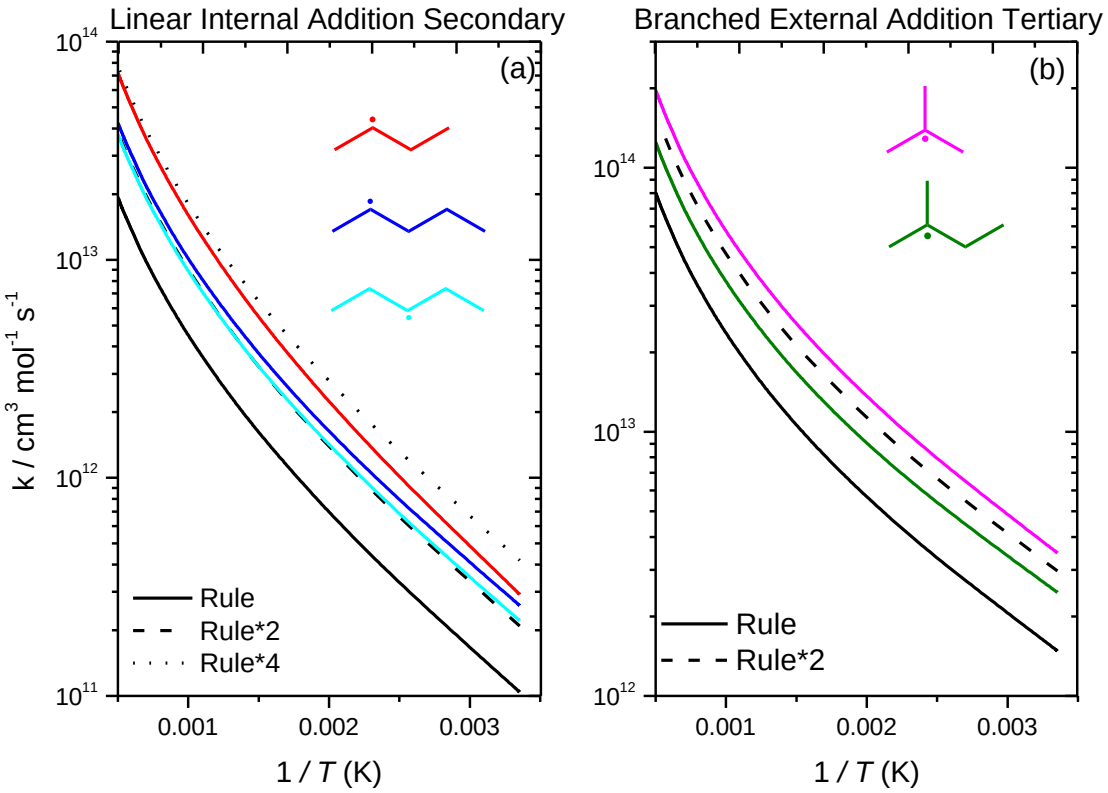

Figure 9. Examples of the application of the proposed rules for Ḣ atom addition to alkenes.

Figure 9 illustrates an example of the rules proposed for (a) internal Ḣ addition to a linear alkene forming a secondary radical and (b) external addition to a branched alkene forming a tertiary radical. The rule is represented by a black solid line. Factors of two and four variations in the rule are represented by dashed and dotted lines, respectively. The coloured lines represent the symmetry corrected rate constants for each respective reaction, with the uncertainty bounds

presented in Table 7. Presented in Fig. 9(a) are the recommended rate constants (symmetry uncorrected) which is multiplied by four for C_4H_8-2 + Ḣ ↔ $\dot{C}_4H_9$-2 since the reactant has a symmetry factor of two and the transition state has a symmetry factor of 0.5. For C_5H_{10}-2 + Ḣ ↔ $\dot{C}_5H_{11}$-2 and C_5H_{10}-2 + Ḣ ↔ $\dot{C}_5H_{11}$-3, the rule is multiplied by two, since the reactant has a symmetry factor of one, and both TSs have a symmetry factor of 0.5. As mentioned earlier, Table S1 of SM presents the symmetry factors for reactants and transition states prior to changing them to one. It was found that this change decreased each Ḣ atom addition rate constant for both linear and branched alkenes by a factor of two, with the exception of C_4H_8-2 + Ḣ ↔ $\dot{C}_4H_9$-2, which is explained above.

3.2.1 Branching ratios of terminal/internal Ḣ atom addition to linear and branched alkenes

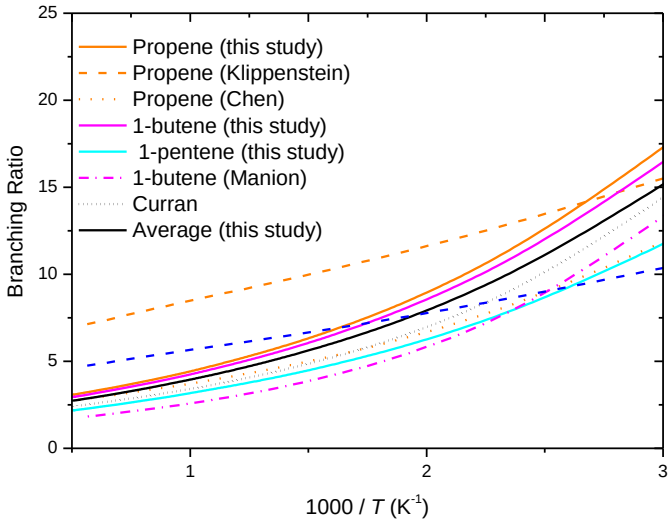

Figure 10. Branching ratio for terminal to internal Ḣ atom addition to (a) linear and (b) branched 1-alkenes.

As discussed earlier, Manion et al.[9] carried out a shock-tube study to investigate the kinetics of terminal and internal Ḣ atom addition to 1-butene. They observed a factor of three discrepancy in the branching ratio for terminal/internal Ḣ atom addition compared to that calculated by Miller and Klippenstein[7] for the Ḣ + propene reactions. Manion et al.[9] state that the difference is well outside the experimental error of their experiments or the expected differences for 1-butene. One of the aims of the current work is thus to investigate the branching ratio of terminal to internal Ḣ atom addition in 1-alkenes. Branching ratios for Ḣ atom addition to linear 1-alkenes for $C_2 - C_5$ alkenes are plotted in Fig. 10. The branching ratios for propene

and 1-butene calculated in the current work are within 5% of each other while our calculated branching ratio for 1-pentene is approximately 40 – 48% lower than that for propene. Non-terminal addition to pentene is ~1.33 – 1.92 times faster than that for propene and 1-butene at $T < 300$ K. However, terminal addition to propene and 1-butene is 1.2 – 1.38 times faster than for 1-pentene at $T > 1000$ K. The solid black line represents an average of the calculated rate constants for external addition to a linear 1-alkene forming a secondary radical to internal addition to a linear alkene forming a primary radical and is in excellent agreement with Curran's recommendation,[57] with the branching ratios being within 10% of each other. This average branching ratio is also in good agreement with Manion's branching ratio for 1-butene and is within a factor of 1.57 at 2000 K. The dashed blue line is the branching ratio for terminal/non-terminal addition if the rate constant for terminal addition by Miller and Klippenstein[7] was reduced by a factor of 1.5. This adjusted branching ratio still differs with that of Manion's by a factor of ~2.6 and a factor of 1.5 – 2.0 of the branching ratios calculated in the current work at 2000 K.

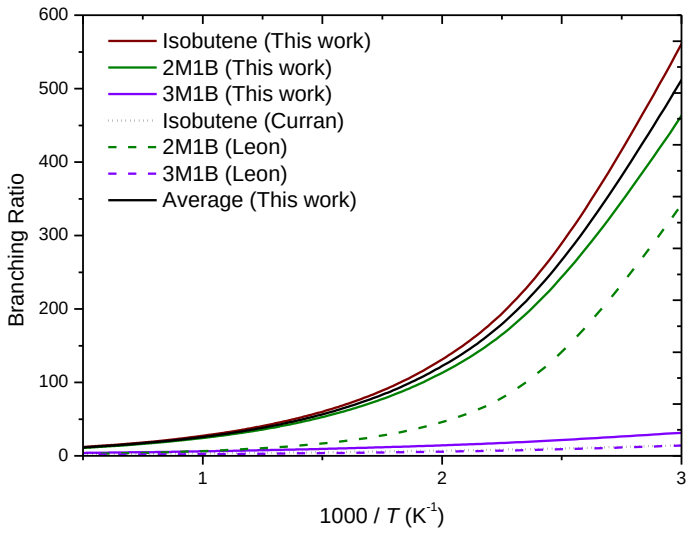

Figure 11. Branching ratio for terminal to internal Ḣ-atom addition to branched 1-alkenes.

Figure 11 presents branching ratios for terminal to internal Ḣ atom addition to branched 1-alkenes. 2-methyl-1-butene (2M1B) and isobutene have a branching ratio of 24.2 and 27.2, respectively at 1000 K. These branching ratios are significantly higher than 3-methyl-1-butene, where the branching ratio of terminal to internal Ḣ atom addition is 6.21 at 1000 K. This is due to branching at the position of the double bond. This results in terminal addition to 2M1B and isobutene forming a tertiary radical, which is more stable than a secondary radical formed through terminal addition to 3M1B, resulting in faster rate constants for terminal addition.

Again, the solid black line represents the branching ratio of our recommended rate constants of external addition to branched 1-alkene forming a tertiary radical to internal addition to a branched alkene forming a primary radical. As mentioned earlier, large deviations in rate constants for isobutene are observed between this work and the recommendations by Curran,[57] particularly for internal Ḣ atom addition. However, Curran does state that no experimental studies for internal Ḣ atom addition existed, so the rate constant recommendation was taken as 2.5 times the rate constant of internal Ḣ atom addition to propene. Manion[9] states in his study that their[9] rates should not be applied to 1-olefins that have branching at the double bond position. We also observe that branching at the double bond significantly influences the branching ratio of 1-olefins and explains the difference as why the branching ratio from Curran is lower than that of the current work. Additionally, Manion[9] states that direct information is lacking on the impact of branching removed from the double bond, but they believe it would have a minimal effect, which is also supported by our calculations here, where our calculated branching ratio for 3M1B is 6.21 at 1000 K. Our calculated branching ratios for propene, 1-butene and 1-pentene are 4.42, 4.24 and 3.17, respectively at 1000 K.

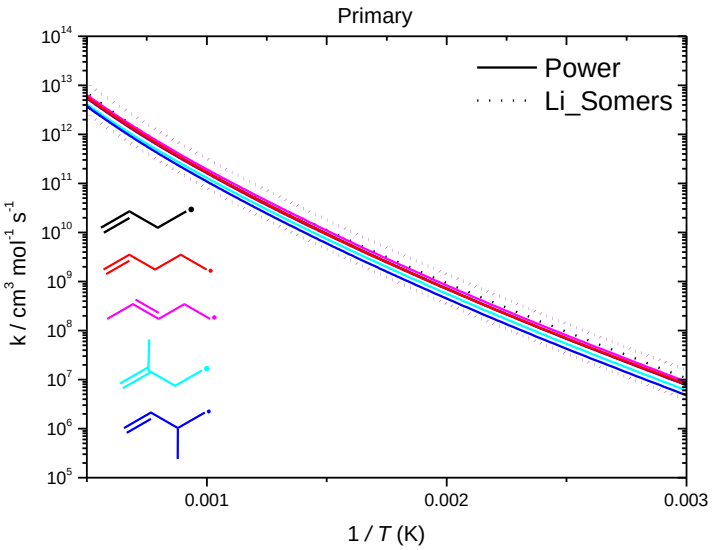

Figure 12. High-pressure limiting rate constants for H-atom abstraction from alkylic (primary) carbon sites on a per Ḣ atom basis.

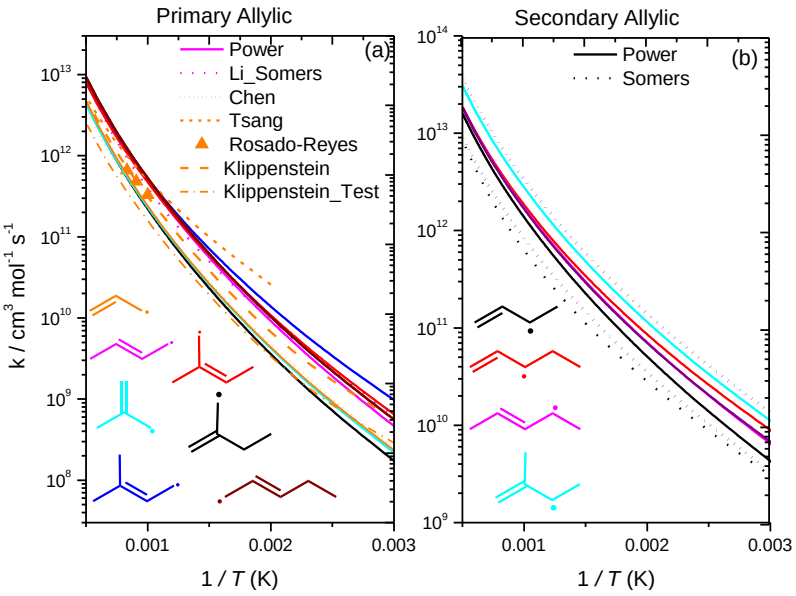

Figure 13. High-pressure limiting rate constants for H-atom abstraction from allylic carbon sites on a per Ḣ atom basis.

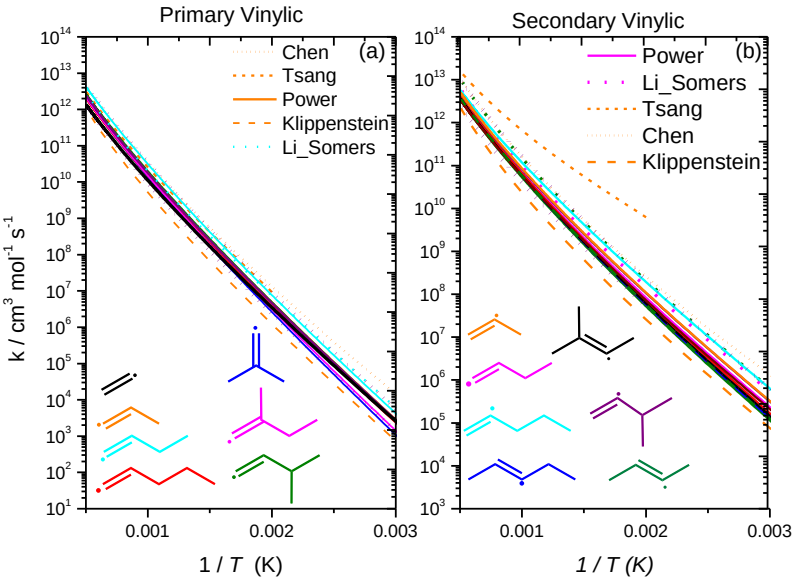

Figure 14. High-pressure limiting rate constants for H-atom abstraction from vinylic carbon sites on a per Ḣ atom basis.

Rate constant comparisons for the H-atom abstraction reactions from C_2-C_4 alkenes were discussed in our previous studies[4-5] on the reactions of Ḣ atoms with the pentene isomers, so we shall be brief here. As mentioned earlier, excellent agreement is observed for H-atom abstraction from the primary carbon sites, Fig. 12. An average of our computed rate constants for abstraction from the primary carbon site as well as the rate calculated by Li et al.[2] is taken as the recommended rate constant. Good agreement is also observed for the abstraction reactions from the primary allylic and vinylic carbon sites.

For H-atom abstraction from the primary allylic carbon sites, a trend was observed in which abstraction from 2-alkenes is faster than that from 1-alkenes, Fig. 13(a). As a result, two rate constant recommendations were proposed. The average energy barriers for abstraction from the primary allylic site of 1-alkenes and 2-alkenes computed in this work are 31.0 and 28.6 kJ mol^{-1}, respectively which accounts for most of the difference observed. The difference observed at higher temperatures can be attributed to the difference in entropy of activation. For the rate constant recommendation for 1-alkenes, an average of the rates calculated in this work and previous studies as well as that by Chen et al.[8] is taken.

For 2-alkenes, an average of our computed rate constants and the rate constant by Li et al.[2] is taken as the recommended value. For comparison purposes, the rate constant calculated by Miller and Klippenstein[7] was decreased by a factor of two since this was another reaction for which they altered the energy barrier. The altered rate constant agrees well with the rate constant calculated in the current work and with that from Chen et al.[8] Moreover, for abstraction from the secondary allylic and primary vinylic carbon site, an average of our calculated rates and that by Li et al.[2] is taken as the recommended rate constant. For abstraction from the secondary vinylic site, an average of our computed rate constants, Li et al., Chen et al. and Miller and Klippenstein is taken.[2,18,20] A factor of two uncertainty is applied to these recommendations and are represented by dotted purple lines in Figs. 12 – 14. For clarity reasons, the factor of two uncertainty is not shown for Fig.13 (a) since there are two recommended rate constants.

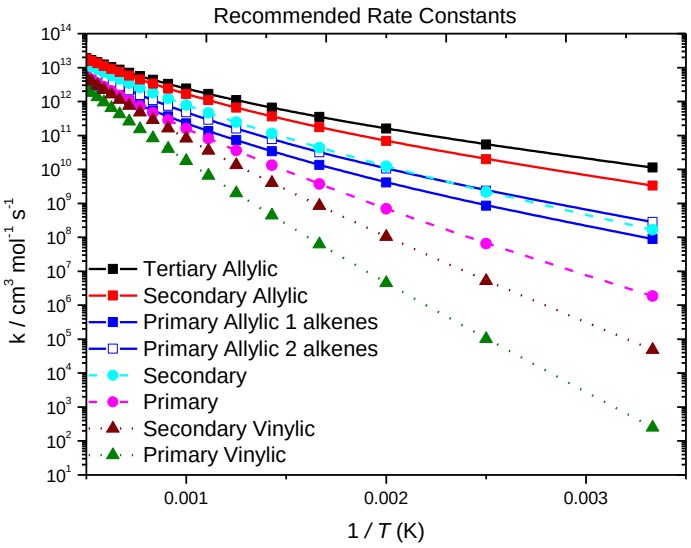

Figure 15. Rate constant recommendations for H-atom abstraction from $C_2 - C_5$ alkenes. Solid (allylic), dashed (alkyl) and dotted (vinylic).

Table 9. Recommended rate constants for H-atom abstraction from alkenes on a per H-atom basis. ($A.T^n$ = cm^3 mol^{-1} s^{-1}, energies = cal mol^{-1}). Fit between 300 and 2000 K.

Class	*A*	*n*	*Ea*	Uncertainty Bounds (Upper, Lower)
Primary	4.69×10^{04}	2.68	6959.	1.42, 1.35
Primary Allylic: 1 alkenes	9.14×10^{02}	3.06	3582.	1.10, 1.28
Primary Allylic: 2 alkenes	1.32×10^{03}	3.08	3203.	1.19, 1.50
Primary Vinylic	2.72×10^{05}	2.54	12819.	2.39, 2.95
Secondary	4.08×10^{05}	2.44	4734.	–
Secondary Allylic	1.06×10^{05}	2.59	2654.	1.67, 2.67
Secondary Vinylic	2.41×10^{05}	2.55	9611.	2.09, 2.02
Tertiary Allylic	2.10×10^{06}	2.19	2329.	–

cm^3 /mol/s/cal units.

3.3 Reactions of alkyl radicals

3.3.1 Ethyl ($\dot{C}_2H_5$) radical

Ethyl radicals are formed via $\dot{H}$ atom addition to ethylene (11.2 kJ mol^{-1}). C–H β-scission of ethyl radicals can also occur with a barrier height of 157.7 kJ mol^{-1}.

Table 10. Computed energy barriers, heats of reaction, and high-pressure limiting rate constant fits for the reactions of $C_3 - C_4$ alkyl radicals. Units (AT^n = s^{-1}, energies = kJ mol^{-1}). Fit between 298 and 2000 K.

Reaction	$\Delta^{\ddagger}H_{0K}$	Δ_rH_{0K}	*A*	*n*	*Ea*
$n\dot{C}_3H_7 \rightleftharpoons i\dot{C}_3H_7$	158.09	–13.86	2.22×10^{05}	2.05	129.83
$n\dot{C}_3H_7 \leftrightarrow C_2H_4 + \dot{C}H_3$	127.91	91.40	1.10×10^{16}	–0.72	135.31
$\dot{C}_4H_9$-1 $\rightleftharpoons$ $\dot{C}_4H_9$-2	162.78	–11.15	8.80×10^{-05}	4.82	111.84
$\dot{C}_4H_9$-1 $\leftrightarrow$ $C_2H_4 + \dot{C}_2H_5$	124.29	89.93	3.64×10^{15}	–0.58	130.33
$\dot{C}_4H_9$-2 $\leftrightarrow$ $C_3H_6 + \dot{C}H_3$	129.45	93.21	1.87×10^{14}	–0.20	134.93
$i\dot{C}_4H_9 \rightleftharpoons \dot{C}_4H_9$-t	150.21	–21.17	8.08×10^{01}	3.03	116.48
$i\dot{C}_4H_9 \leftrightarrow C_3H_6 + \dot{C}H_3$	129.86	86.81	1.46×10^{17}	–0.91	137.99

3.3.2 Propyl (n$\dot{C}_3H_7$ and i$\dot{C}_3H_7$) radicals

Once n$\dot{C}_3H_7$ radicals are formed via internal Ḣ atom addition to propene, they can undergo C–C β-scission to form ethylene and $\dot{C}H_3$ radicals with an energy barrier of 127.9 kJ mol^{-1}, (Table 10) which is more favourable (by 30.2 kJ mol^{-1}) than isomerisation to i$\dot{C}_3H_7$ radicals. They can also undergo C–H β-scission, with an energy barrier of 148.6 kJ mol^{-1}. The i$\dot{C}_3H_7$ radicals formed can undergo a Ḣ atom elimination reaction, with an energy barrier of 155.2 kJ mol^{-1}.

3.3.3 Butyl ($\dot{C}_4H_9$-1 and $\dot{C}_4H_9$-2) radicals

$\dot{C}_4H_9$-1 radicals are formed via internal Ḣ atom addition to 1-butene, while terminal addition leads to the formation of $\dot{C}_4H_9$-2 radicals. $\dot{C}_4H_9$-2 radicals are also formed through internal Ḣ atom addition to 2-butene. C–C β-scission of $\dot{C}_4H_9$-1 radicals can occur forming ethylene and $\dot{C}_2H_5$ radicals, with a barrier height of 124.3 kJ mol^{-1}, which is more favourable (by 33.5 kJ mol^{-1}) than isomerisation to $\dot{C}_4H_9$-2 radicals. Additionally, C–H β-scission of $\dot{C}_4H_9$-1 radicals can occur with a barrier height of 152.5 kJ mol^{-1}. Two transition states are available for the reaction $\dot{C}_4H_9$-1 ⇌ $\dot{C}_4H_9$-2, one occurring through a 3-membered ring and the second one occurring through a 4-membered ring, with barrier heights of 160.6 and 162.8 kJ mol^{-1}, respectively. C–C β-scission of $\dot{C}_4H_9$-2 can also occur, forming propene and a $\dot{C}H_3$ radical, with an energy barrier of 129.45 kJ mol^{-1}, while C–H β-scission of $\dot{C}_4H_9$-2 has a barrier height of 148.6 kJ mol^{-1}.

3.3.4 Branched butyl (i$\dot{C}_4H_9$ and t$\dot{C}_4H_9$) radicals

Internal Ḣ atom addition to isobutene forms i$\dot{C}_4H_9$ radicals, while terminal addition forms t$\dot{C}_4H_9$ radicals. C–H β-scission of i$\dot{C}_4H_9$ radicals can occur, with a barrier height of 145.6 kJ mol^{-1}. However, C–C β-scission of i$\dot{C}_4H_9$ radicals, forming propene and $\dot{C}H_3$ radicals is more favoured, with a reaction barrier of 129.9 kJ mol^{-1}. Isomerisation of i$\dot{C}_4H_9$ to t$\dot{C}_4H_9$ occurs with a higher energy barrier of 150.2 kJ mol^{-1}. C–H β-scission of t$\dot{C}_4H_9$ can occur, with a barrier height of 151.7 kJ mol^{-1}.

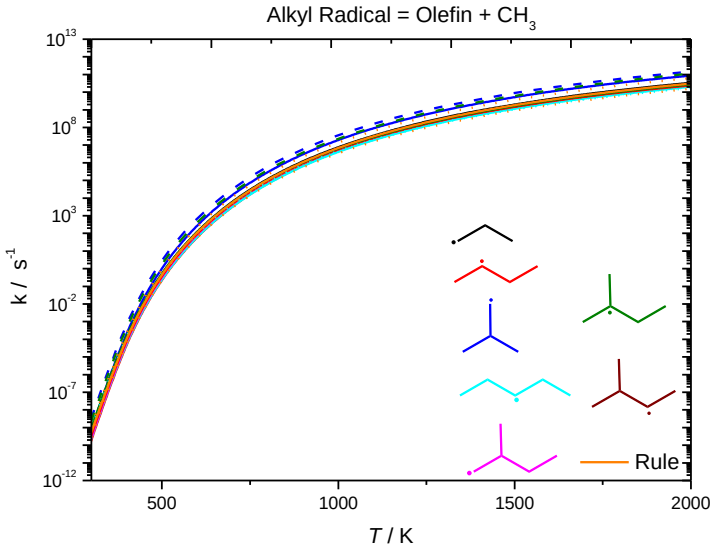

Figure 16. High-pressure limiting rate constants for alkyl radical decomposition, forming (a) olefin + $\dot{C}H_3$. Solid (current work), dashed (Curran), dotted (Awan) and short-dotted (Comandini).

Figure 16 presents high-pressure limiting rate constants for alkyl radical decomposition reactions forming an olefin + $\dot{C}H_3$. For comparison, rate constants for alkyl radical decomposition from our previous work on C_5 alkenes in addition to other literature sources[4, 57, 59-61] are plotted. The rate constant for the reaction $i\dot{C}_4H_9 \leftrightarrow C_3H_6 + \dot{C}H_3$ recommended by Curran[57] is a factor of 2.74 – 1.67 times faster than that calculated in this work in the temperature range 500 – 2000 K. With the exception of this reaction, all other rate constants calculated in this work for alkyl radicals leading to the formation of an olefin and a $\dot{C}H_3$ radical are within a factor of 1.55 of our computed rate constant for $n\dot{C}_3H_7 \leftrightarrow C_2H_4 + \dot{C}H_3$ over the temperature range 298 – 2000 K. The rate constant calculated in this work for $i\dot{C}_4H_9 \leftrightarrow C_3H_6 + \dot{C}H_3$ is a factor of 2.54 – 3.08 times faster than $n\dot{C}_3H_7 \leftrightarrow C_2H_4 + \dot{C}H_3$. This may be due to the fact that $i\dot{C}_4H_9$ radicals have three degenerate sites for C–C β-scission to take place.

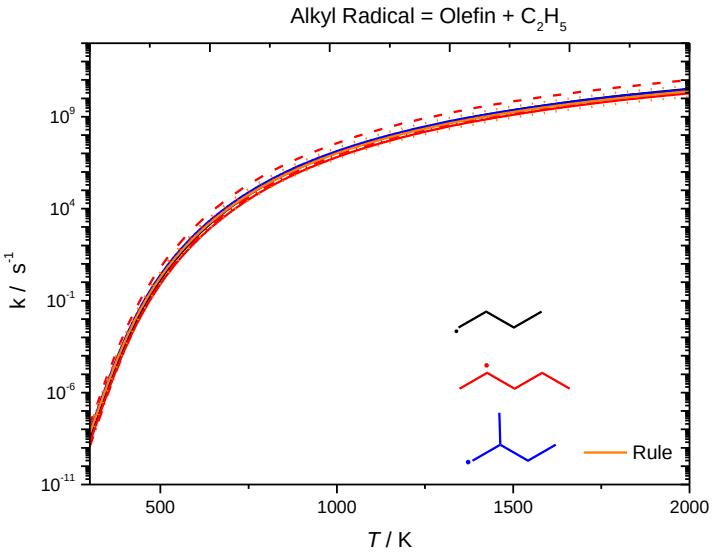

Figure 17. High-pressure limiting rate constants for alkyl radical decomposition, forming an olefin + $\dot{C}_2H_5$. Solid (current work), dashed (Curran), dotted (Awan), short-dotted (Comandini), and dashed-dotted (Jitariu).

Reasonable agreement is observed for the reactions of alkyl radicals forming an olefin and $\dot{C}_2H_5$ radicals calculated previously and in this work. In Fig.17, the rate constant recommendation by Curran[57] for the reaction $\dot{C}_5H_{11}$-2 ↔ C_3H_6 + $\dot{C}_2H_5$ is the fastest in comparison to the other analogous reactions. The Curran recommendation[57] is a factor of ~9.5 – 5.0 times faster than our calculated rate constant for $\dot{C}_5H_{11}$-2 ↔ C_3H_6 + $\dot{C}_2H_5$ calculated previously over the temperature range 300 – 2000 K [4]. The value from Awan and Comandini[59-60] is a factor of ~3.4 times faster than our previous work[4] for the same reaction at 500 K, with the rate constants converging at higher temperatures. Jitariu et al.[61] are in excellent agreement with our previous work for the reaction $\dot{C}_5H_{11}$-2 ↔ C_3H_6 + $\dot{C}_2H_5$,[4] with the rate constants being within a factor of ~1.3. The rate constant for the reaction a$\dot{C}_5H_{11}$ ↔ C_3H_6 + $\dot{C}_2H_5$ calculated in our most recent study[5] is a factor of ~3 times faster at 500 K than our calculated rate constant for $\dot{C}_5H_{11}$-2 ↔ C_3H_6 + $\dot{C}_2H_5$.[4] An energy barrier difference of 1.9 kJ mol^{-1} accounts for a factor of 1.6 of this difference. For the decomposition of an alkyl radical forming an olefin and an ethyl radical, an average of the rate constants calculated in our current and previous studies [4-5] as well as those by Awan, Comandini and Jitariu[4, 57, 59-61] is taken, with a factor of two of the recommended represented as orange dotted lines.

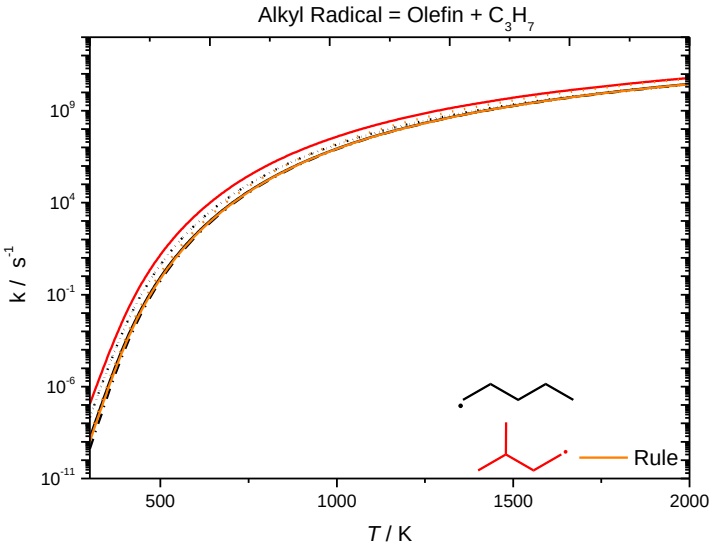

Figure 18. High-pressure limiting rate constants for alkyl radical decomposition, forming an olefin + $\dot{C}_3H_7$. Solid (current work), dotted (Awan), short-dotted (Comandini), and dashed-dotted (Jitariu).

Figure 18 presents rate constant comparisons for alkyl radical decomposition forming an olefin and propyl radicals. The reactions $\dot{C}_5H_{11}$-1 ↔ C_2H_4 + n$\dot{C}_3H_7$ and d$\dot{C}_5H_{11}$ ↔ C_2H_4 + i$\dot{C}_3H_7$ are plotted for comparison. The rate constants for the reaction $\dot{C}_5H_{11}$-1 ↔ C_2H_4 + n$\dot{C}_3H_7$ by Awan,[59] Comandini[60] and Jitariu et al.[61] are in good agreement with our previously calculated rate constant.[4] At 500 K, the values from Awan[59] and Comandini[60] are a factor of ~4.5 times faster than our calculated rate constant for this reaction at 500 K, with the rate constants converging at high temperatures. The difference of 7.76 kJ mol^{-1} in the energy barrier accounts for the observed difference. Larger differences are observed between the values calculated in this work and by Awan and Comandini at temperatures below 500 K, therefore the recommended rate constant for $\dot{C}_5H_{11}$-1 ↔ C_2H_4 + n$\dot{C}_3H_7$ is taken as an average of the rate calculated in the current work and by Jitariu et al.[61] The rate constant by Jitariu et al. is in excellent agreement with our calculated rate constant for the same reaction.[4] Our calculated rate constant for d$\dot{C}_5H_{11}$ ↔ C_2H_4 + i$\dot{C}_3H_7$ is also plotted in this graph, which is taken as the recommended rate constant for alkyl radical decomposition forming an olefin and an i$\dot{C}_3H_7$ radical.

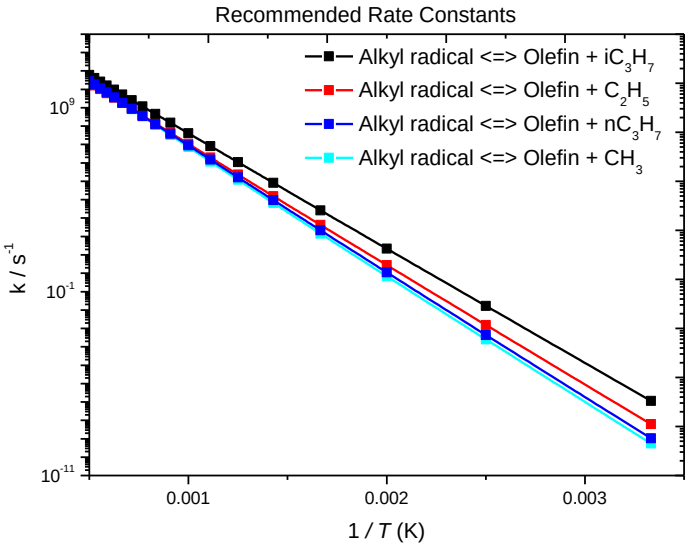

Figure 19. Rate constant recommendations for alkyl radical decomposition to olefin + radical.

Table 11. Recommended rate constants for alkyl radical decomposition forming an olefin + radical. (AT^n = s^{-1}, energies = cal mol^{-1}). Fit between 300 K and 2000 K.

Class	*A*	*n*	*Ea*	Uncertainty Bounds (Upper, Lower)
alkyl radical ↔ olefin + $\dot{C}H_3$	2.54×10^{10}	1.04	30573.	2.86, 3.71
alkyl radical ↔ olefin + $\dot{C}_2H_5$	5.20×10^{11}	0.57	29308.	1.34, 3.11
alkyl radical ↔ olefin + $n\dot{C}_3H_7$	9.62×10^{11}	0.55	30678.	1.61, 2.60
alkyl radical ↔ olefin + $i\dot{C}_3H_7$	6.87×10^{12}	0.31	28225.	–

4.0 Detailed kinetic modeling

All simulations were performed using Chemkin-Pro assuming a constant volume homogeneous batch reactor. As described in our previous study of the pentene isomers,[5] test computations implied that the high-pressure limiting rate constant for external Ḣ atom addition to 2M1B was over-estimated by a factor of 2 – 3, which is also in line with the variational effect observed by Jasper and Hansen[62] for Ḣ atom addition to large molecular weight species. To assess the influence of variational effects on predictions of experimental data, indicative simulations are carried out by systematically reducing the rate constants for Ḣ atom addition by a factor of two in the RRKM/ME model and re-computing $k(T,p)$. The approximate

variational calculation results from the current work for the alkene + Ḣ systems have been included in NUIGMech1.1 which includes our results from our previous studies of the pentene isomers.[4-5] The updated model, NUIGMech1.2, is used to simulate the recent results from a pyrolysis study of 1-alkenes using the NUIG single pulse shock-tube[31] and is represented by solid lines. Dashed lines represent model predictions of NUIGMech1.1. The updates to the pyrolysis reactions between the two models is solely from the present work. Improvements in species mole fractions are observed, particularly for 2-butene and isobutene pyrolysis.[33] The supporting information contains PLOG fits for both the approximate variational results and the original unadjusted results.

4.1 Ethylene pyrolysis

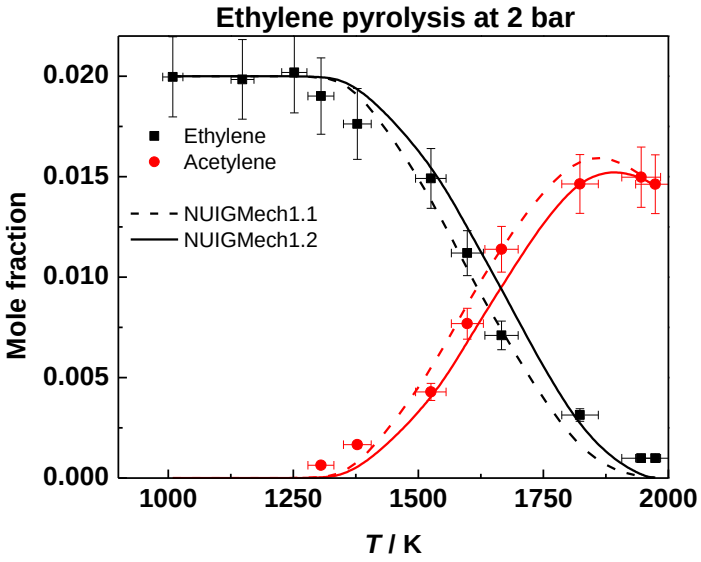

Figure 20. Species profiles for ethylene pyrolysis at 2 bar. Dashed lines represent NUIGMech1.1 and solid lines represent NUIGMech1.2.

Figure 20 presents species profiles for ethylene pyrolysis at 2 bar.[31] The reaction path analysis was already described by Nagaraja et al.[31] so we shall be brief here. H-atom abstraction by Ḣ atoms from ethylene leads to the production of vinyl radicals, with vinyl radicals decomposing to acetylene + Ḣ. Through the incorporation of the rate constants calculated in this work (NUIGMech1.2), there is a slight improvement in the species profiles for both ethylene and acetylene. The rate constant for H-atom abstraction from ethylene is approximately a factor of two slower, which reduces the amount of vinyl radical produced, which in turn decreases the production of acetylene and Ḣ atoms.

4.2 Propene pyrolysis

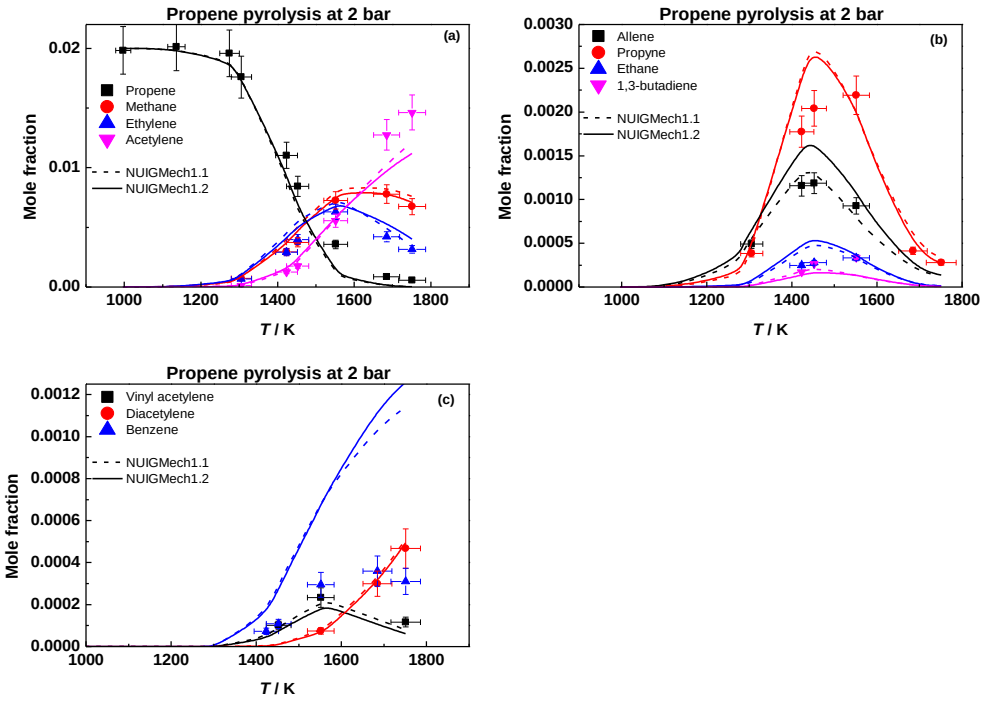

Figure 21. Species profiles for propene pyrolysis at 2 bar. Dashed lines represent NUIGMech1.1 and solid lines represent NUIGMech1.2.

Figure 21 presents species profiles for propene pyrolysis at 2 bar.[31] Both Ḣ atom addition and abstraction reactions are the main consumption pathways for propene. Ḣ atom addition to propene and the subsequent decomposition of propyl radical, leads to the formation of ethylene and a methyl radical. Abstraction of an allylic H-atom by Ḣ atoms or $\dot{C}H_3$ radicals leads to the formation of allyl and H_2 and CH_4. Allyl radicals are converted to allene, which subsequently isomerises to propyne or undergoes H-atom abstraction to form propargyl radicals, which in turn produces benzene. Acetylene is formed by the decomposition of vinyl radicals, the reaction of Ḣ atoms with allene and propyne, and the β-scission of propen-1-yl radical.

4.3 1-Butene pyrolysis

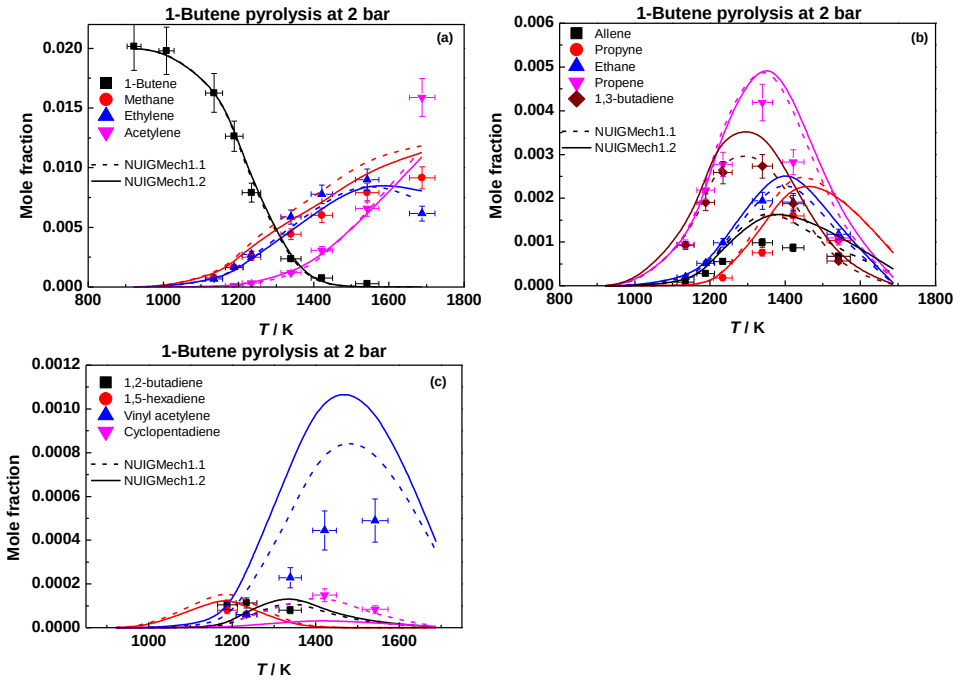

Figure 22. Species profiles for 1-butene pyrolysis at 2 bar. Dashed lines represent NUIGMech1.1 and solid lines represent NUIGMech1.2

Figure 22 presents species profiles for 1-butene pyrolysis at 2 bar.[31] The pyrolysis chemistry is quite similar to that of propene, with both Ḣ atom addition and abstraction reactions being important pathways. H-atom addition to 1-butene produces propene and a $\dot{C}H_3$ radical and ethylene and a $\dot{C}_2H_5$ radical via two chemically activated pathways. Ethyl radicals decompose to ethylene + Ḣ. Hydrogen atom abstraction by Ḣ or $\dot{C}H_3$ leads to the formation of $\dot{C}_4H_7$1-3, which in turn forms 1,3-butadiene. Methane is formed primarily by H-atom abstraction by $\dot{C}H_3$ radicals from the fuel and other stable species. Acetylene is mainly produced by the decomposition of vinyl radicals and the reactions of Ḣ atoms with allene and propyne.

4.4 Trans 2-butene pyrolysis

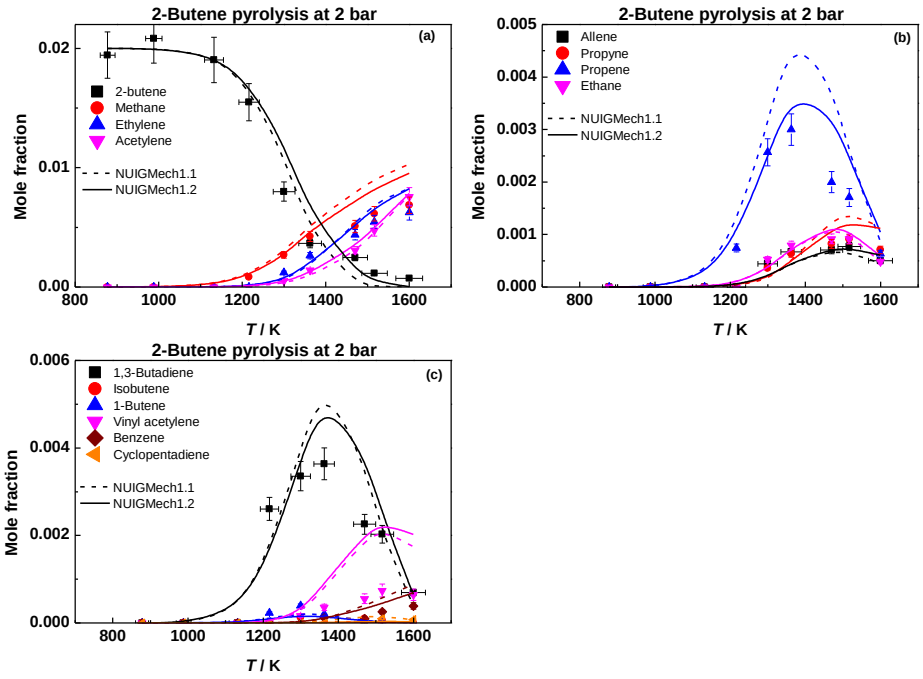

Figure 23. Species profiles for 2-butene pyrolysis at 2 bar. Dashed lines represent NUIGMech1.1 and solid lines represent NUIGMech1.2.

Figure 23 presents species profiles for 2-butene pyrolysis at 2 bar.[33] Again, the pyrolysis chemistry is quite similar to that of propene and 1-butene. Ḣ atom addition to 2-butene forms propene and $\dot{C}H_3$ radicals through a chemically activated pathway. H-atom abstraction by Ḣ or $\dot{C}H_3$ leads to the formation of $\dot{C}_4H_7$1-3, which in turn forms 1,3-butadiene. The rate constant for H-atom abstraction from 2-butene forming $\dot{C}_4H_7$1-3 calculated in this work is a factor of 2.5 times slower than that used in NUIGMech1.1, which in turn reduces the species mole fraction of 1,3-butadiene. For the propene species profiles, there is an improvement in the predictions through the incorporation of the calculations computed in the current work. The production of propene, as previously stated comes from the chemically activated pathway of Ḣ atom addition to 2-butene. The rate constants in NUIGMech1.1 are based on QRRK/MSC estimates and are approximately a factor of ~seven times faster than those in NUIGMech1.2 at 1400 K. Again, methane is mainly produced by H-atom abstraction by $\dot{C}H_3$ from the fuel and other stable species. Acetylene is mainly produced by the decomposition of vinyl radicals and the reactions of Ḣ atoms with allene and propyne.

4.5 Isobutene pyrolysis

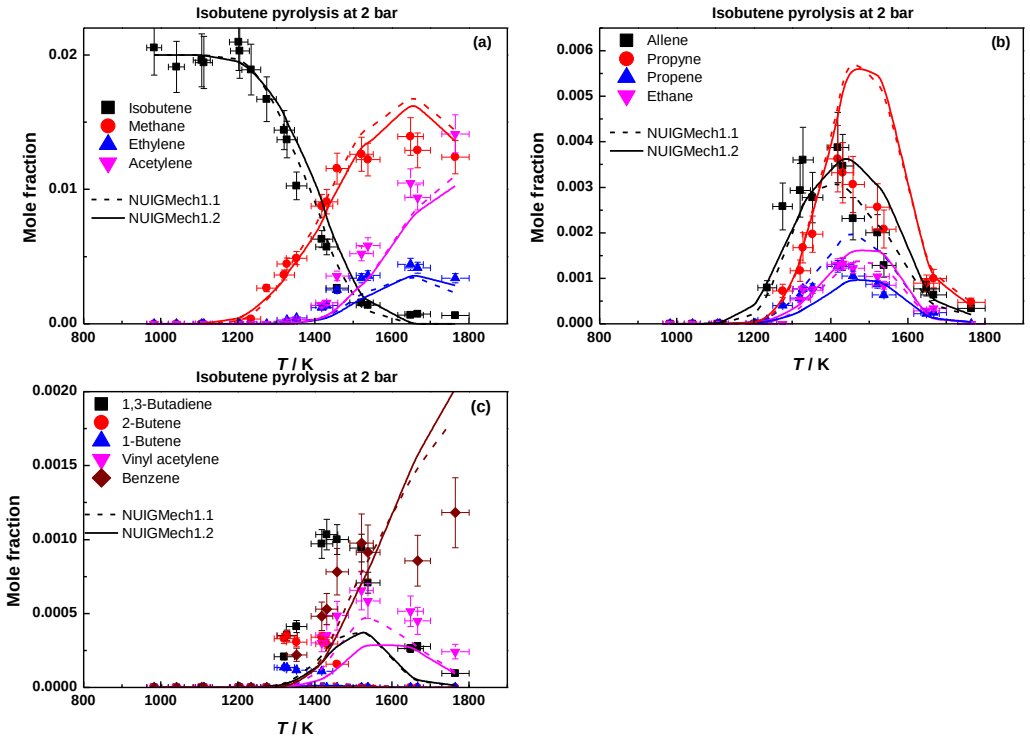

Figure 24. Species profiles for isobutene pyrolysis at 2 bar. Dashed lines represent NUIGMech1.1 and solid lines represent NUIGMech1.2.

Figure 24 presents species profiles for isobutene pyrolysis at 2 bar.[33] Ḣ atom abstraction from isobutene leads to the formation of i$\dot{C}_4H_7$ radicals, which decompose to produce allene and $\dot{C}H_3$ radicals. The resulting allene then isomerises to propyne. Propene is primarily formed through the chemically activated pathway of Ḣ atom reaction to isobutene. There is an improvement in the propene predictions with the current model, due to the rate constant for the chemically activated pathway of Ḣ atom addition to isobutene being approximately a factor of seven times slower at 1400 K.

5.0 Chemically activated pathways

5.1 Effect of pressure

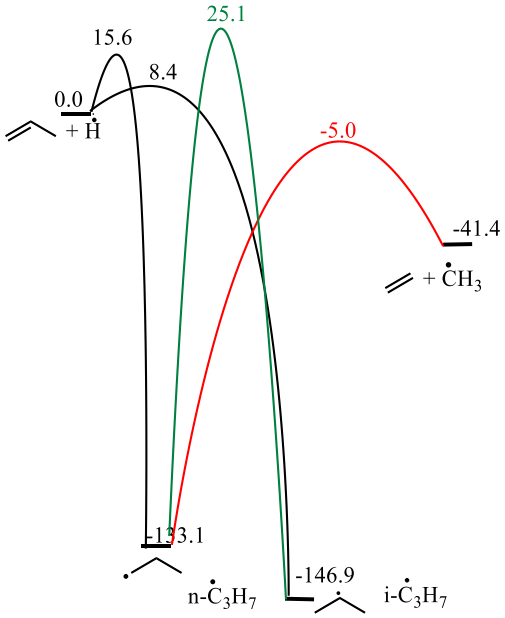

Figure 25. Potential energy surface for Ḣ-atom addition reactions of propene. Energies in kJ mol^{-1}.

From the simulations, it is observed that the chemically activated pathways for the reaction of Ḣ atoms with alkenes are important in capturing the species profiles of the products during pyrolysis and oxidation. Taking propene as an example, which is described in Figure 4 above, the formation of stabilised iC_3H_7 radicals through the reaction of Ḣ atoms with propene dominates at temperatures up to 800, 1000, 1200, and 1500 at pressures of 0.1, 1, 10, and 100 atm respectively. The chemically activated pathway $C_3H_6 + Ḣ \leftrightarrow [nC_3H_7]^* \leftrightarrow C_2H_4 + ĊH_3$ then dominates the reaction flux at higher temperatures. At 1000 atm, the formation of stabilised iC_3H_7 radicals dominates over the entire temperature range.

At 1000 K and 0.1 atm, 70% of the reaction flux goes through this chemically activated pathway for $C_3H_6 + Ḣ$. However, as the pressure increases, this percentage reduces, and the stabilisation reaction channel becomes more favourable. The percentage reaction flux going through this chemically activated pathway is 41%, 20%, 7% and 2% for pressures of 1, 10, 100, and 1000 atm respectively. It is therefore important to have accurate rate constants for the chemically activated pathways on these potential energy surfaces in order to predict the species mole fractions across a wide range of temperatures and pressures. Below are a list of some of the chemically activated pathways forming some of the major products of pyrolysis calculated in the current study and in previous ones.[4,5]

- $C_3H_6 + \dot{H} \leftrightarrow [n\dot{C}_3H_7]^* \leftrightarrow C_2H_4 + \dot{C}H_3$
- $C_4H_8\text{-}1 + \dot{H} \leftrightarrow [\dot{C}_4H_9\text{-}1]^* \leftrightarrow C_2H_4 + \dot{C}_2H_5$
- $C_4H_8\text{-}1 + \dot{H} \leftrightarrow [\dot{C}_4H_9\text{-}2]^* \leftrightarrow C_3H_6 + \dot{C}H_3$
- $C_4H_8\text{-}2 + \dot{H} \leftrightarrow [\dot{C}_4H_9\text{-}2]^* \leftrightarrow C_3H_6 + \dot{C}H_3$
- $iC_4H_8 + \dot{H} \leftrightarrow [i\dot{C}_4H_9]^* \leftrightarrow C_3H_6 + \dot{C}H_3$

Moreover, chemically activated pathways were also found to be important for the reactions of $\dot{H}$ with the pentene isomers in our previous studies.[4,5]

- $C_5H_{10}\text{-}1 + \dot{H} \leftrightarrow [\dot{C}_5H_{11}\text{-}1]^* \leftrightarrow C_2H_4 + n\text{-}\dot{C}_3H_7$
- $C_5H_{10}\text{-}1 + \dot{H} \leftrightarrow [\dot{C}_5H_{11}\text{-}2]^* \leftrightarrow C_3H_6 + \dot{C}_2H_5$
- $C_5H_{10}\text{-}2 + \dot{H} \leftrightarrow [\dot{C}_5H_{11}\text{-}2]^* \leftrightarrow C_3H_6 + \dot{C}_2H_5$
- $C_5H_{10}\text{-}2 + \dot{H} \leftrightarrow [\dot{C}_5H_{11}\text{-}3]^* \leftrightarrow C_4H_8\text{-}1 + \dot{C}H_3$
- $aC_5H_{10} + \dot{H} \leftrightarrow [a\dot{C}_5H_{11}]^* \leftrightarrow C_3H_6 + \dot{C}_2H_5$
- $aC_5H_{10} + \dot{H} \leftrightarrow [a\dot{C}_5H_{11}]^* \leftrightarrow C_4H_8\text{-}1 + \dot{C}H_3$
- $aC_5H_{10} + \dot{H} \leftrightarrow [b\dot{C}_5H_{11}]^* \leftrightarrow iC_4H_8 + \dot{C}H_3$
- $bC_5H_{10} + \dot{H} \leftrightarrow [b\dot{C}_5H_{11}]^* \leftrightarrow iC_4H_8 + \dot{C}H_3$
- $bC_5H_{10} + \dot{H} \leftrightarrow [c\dot{C}_5H_{11}]^* \leftrightarrow C_4H_8\text{-}2 + \dot{C}H_3$
- $cC_5H_{10} + \dot{H} \leftrightarrow [c\dot{C}_5H_{11}]^* \leftrightarrow C_4H_8\text{-}2 + \dot{C}H_3$
- $cC_5H_{10} + \dot{H} \leftrightarrow [d\dot{C}_5H_{11}]^* \leftrightarrow C_2H_4 + i\dot{C}_3H_7$

5.2 Effect of molecular size

As the size of the molecule increases from propene to 1-butene, the effect of chemical activation becomes greater, especially at lower pressures. At 1000 K and 0.1 atm, for 1-butene 99% of the reaction flux proceeds through the chemically activated pathways compared to 70% for propene.

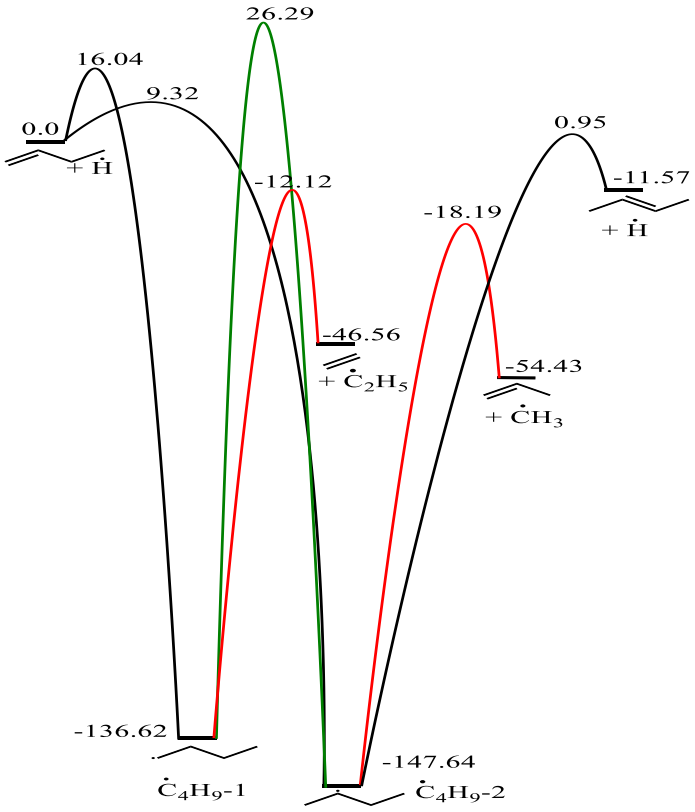

Figure 26. Potential energy surface for Ḣ-atom addition reactions of 1- and 2-butene. Energies in kJ mol^{-1}.

For the pentene isomers, it was shown that > 95% of the reaction flux proceeds through the chemically activated pathways at 1000 K and 0.1 atm,[4,5] which is similar to butene. As the pressure increases, this percentage reduces to 93%, 65%, 25% and 4% at pressures of 1, 10, 100, and 1000 atm, respectively for 1-butene, compared to 41%, 20%, 7% and 2% for propene. The formation of stabilised Ċ$_4$H$_9$-2 radicals through the reaction of Ḣ atoms with 1-butene then dominates, which can be seen in Figure 6(a). A similar situation prevails for 2-butene, Figure 6(b) where 98%, 87%, 57%, 20% and 3% proceeds through chemical activation at 0.1, 1, 10, 100 and 1000 atm. In the case of isobutene, 33% of the reaction flux goes through the chemically activated pathways at 1000 K and 0.1 atm, with the formation of stabilised tĊ$_4$H$_9$ radicals then dominating the reaction flux. It is not until a temperature of 1200 K is reached that chemical activation is considerable, accounting for 74% at 0.1 atm, Figure 6(c). It is observed that the effect of chemical activation becomes greater as the molecular size increases from propene to butene. However, as the molecular size increases from butene to pentene the effect of chemical activation is similar.

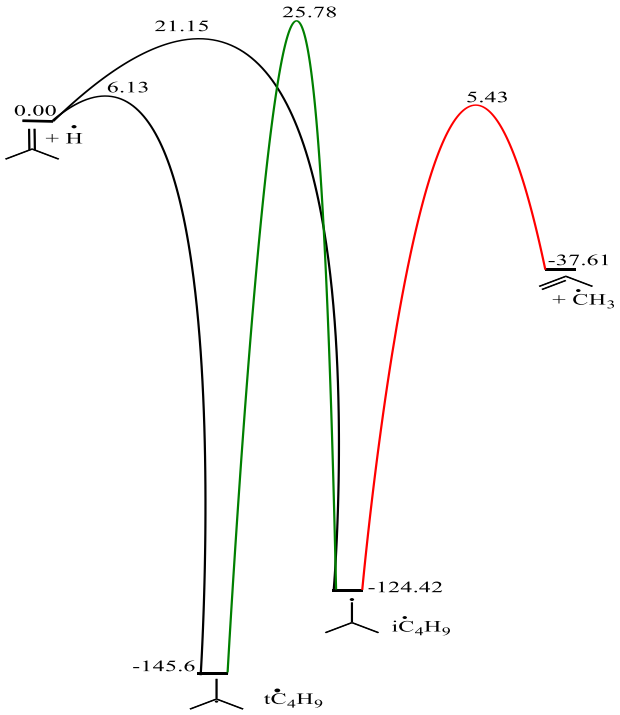

Figure 27. Potential energy surface for Ḣ-atom addition reactions of isobutene. Energies in kJ mol^{-1}.

Conclusions

To contribute to the development of combustion models, a hierarchical set of rate constants for the reactions of Ḣ atom with $C_2 - C_5$ alkenes, and the subsequent C–C and C–H β-scission and Ḣ atom transfer reactions using the same level of theory now exist. The reactions for the linear and branched C_5 alkenes were performed in our previous studies, while calculations for $C_2 - C_4$ species are performed in the current work. Thermochemical data are calculated as a function of temperature, with enthalpies of formation determined from an isodesmic network, which is built upon benchmark literature data and electronic structure calculations. High-pressure limiting and temperature- and pressure-dependent rate constants are calculated using RRKM theory with a 1-D master equation (ME) analysis. Rate constant recommendations for Ḣ atom addition/abstraction and alkyl radical decomposition are proposed and serve as a useful tool in mechanisms for larger alkenes for which calculations do not exist.

As mentioned in our earlier work,[5] test computations implied that the high-pressure limiting rate constant for Ḣ atom addition were over-estimated by a factor of $2-3$, which is also in line with the variational effect observed by others for Ḣ atom addition reactions to large molecular weight species.[62] To determine the influence of variational effects on model predictions,

indicative simulations are carried out by systematically reducing the rate constants for Ḣ atom addition by a factor of two in the RRKM/ME model and re-computing $k(T,p)$. Similarly to our earlier work [5], it is found that the chemically activated pathways for Ḣ atom addition to alkenes, as well as their abstraction reactions, are found to be important in capturing the species profiles of the products from pyrolysis. Although good agreement is observed between our model predictions and experiment, future work should consider to address VTST, the treatment of multi-dimensional torsions, and an-harmonic effects with the aim of developing a more comprehensive RRKM/ME model for combustion modeling.

Supporting Information

MESS input and output files, thermochemical values in NASA polynomial format and Chemkin format PLOG rate constant fits are provided in the supporting information.

Acknowledgements

The authors acknowledge the support of Science Foundation Ireland in funding this project under Grant 15/IA/3177 and also to the Irish Centre for High-End Computing, ICHEC, under project numbers ngche058c and ngche080c.

Author Contributions

Jennifer Power: Performed electronic structure calculations, modelling work and wrote the manuscript.

Kieran. P. Somers: Performed electronic structure calculations and provided input for theoretical and modelling work.

Shashank. S. Nagaraja: Performed pyrolysis experiments.

Henry. J. Curran: Managed the project throughout and reviewed the manuscript prior and post review process.

Conflicts of Interest Statement

Conflicts of interest: None

References

1. Burke, S. M.; Metcalfe, W.; Herbinet, O.; Battin-Leclerc, F.; Haas, F. M.; Santner, J.; Dryer, F. L.; Curran, H. J. An experimental and modeling study of propene oxidation. Part 1: speciation measurements in jet-stirred and flow reactors. *Combust. Flame* **2014,** *161* (11), 2765-2784.
2. Li, Y.; Zhou, C.-W.; Somers, K. P.; Zhang, K.; Curran, H. J. The oxidation of 2-butene: a high pressure ignition delay, kinetic modeling study and reactivity comparison with isobutene and 1-butene. *Proc. Combust. Inst.* **2017,** *36* (1), 403-411.
3. Zhou, C.-W.; Li, Y.; O'Connor, E.; Somers, K. P.; Thion, S.; Keesee, C.; Mathieu, O.; Petersen, E. L.; DeVerter, T. A.; Oehlschlaeger, M. A.; et al. A comprehensive experimental and modeling study of isobutene oxidation. *Combust. Flame* **2016,** *167*, 353-379.
4. Power, J.; Somers, K. P.; Zhou, C.-W.; Peukert, S.; Curran, H. J. Theoretical, experimental, and modeling study of the reaction of hydrogen atoms with 1- and 2-pentene. *J. Phys . Chem. A* **2019,** *123* (40), 8506-8526.
5. Power, J.; Somers, K. P.; Nagaraja, S. S.; Wyrebak, W.; Curran, H. J. Theoretical study of the reaction of hydrogen atoms with three pentene isomers: 2-methyl-1-butene, 2-methyl-2-butene, and 3-methyl-1-butene. *J. Phys . Chem. A* **2020,** *124*, 10649-10666.
6. Miller, J. A.; Klippenstein, S. J. The H+C_2H_2 (+M)⇄ C_2H_3 (+M) and H+C_2H_2 (+M)⇄ C_2H_5 (+M) reactions: Electronic structure, variational transition-state theory, and solutions to a two-dimensional master equation. *Phy. Chem. Chem. Phys* **2004,** *6* (6), 1192-1202.
7. Miller, J. A.; Klippenstein, S. J. Dissociation of propyl radicals and other reactions on a C_3H_7 potential. *J.Phys.Chem.A* **2013,** *117* (13), 2718-2727.
8. Chen, W. Y.; Nguyen, T. N.; Lin, M. C.; Wang, N. S.; Matsui, H. Experimental and theoretical studies on the reaction of H atom with C_3H_6. *Int. J. Chem. Kinet.* **2020**, *53* (5), 646-659.
9. Manion, J. A.; Awan, I. A. Evaluated kinetics of terminal and non-terminal addition of hydrogen atoms to 1-alkenes: a shock tube study of H+ 1-butene. *J.Phys.Chem.A* **2015,** *119* (3), 429-441.
10. Barker, J. R.; Keil, D. G.; Michael, J.; Osborne, D. T. Reaction H+ C_2H_4: Comparison of three experimental techniques. *J.Chem.Phys* **1970,** *52* (4), 2079-2088.
11. Feng, Y.; Niiranen, J.; Bencsura, A.; Knyazev, V.; Gutman, D.; Tsang, W. Weak collision effects in the reaction C_2H_5 ⇄ C_2H_4 + H. *J.Phys.Chem.A* **1993,** *97* (4), 871-880.
12. Hanning-Lee, M.; Green, N. B.; Pilling, M.; Robertson, S. Direct observation of equilibration in the system H+ C_2H_4⇄ C_2H_5: standard enthalpy of formation of the ethyl radical. *J Phys Chem* **1993,** *97* (4), 860-870.
13. Lee, J.; Michael, J.; Payne, W.; Stief, L. Absolute rate of the reaction of atomic hydrogen with ethylene from 198 to 320 K at high pressure. *J.Chem.Phys* **1978,** *68* (4), 1817-1820.
14. Lightfoot, P. D.; Pilling, M. J. Temperature and pressure dependence of the rate constant for the addition of hydrogen atoms to ethylene. *J. Phys. Chem.* **1987,** *91* (12), 3373-3379.
15. Michael, J.; Osborne, D.; Suess, G. Reaction H+ C_2H_4: Investigation into the effects of pressure, stoichiometry, and the nature of the third body species. *J.Chem.Phys* **1973,** *58* (7), 2800-2806.
16. Pacey, P. D.; Wimalasena, J. H. Kinetics and thermochemistry of the ethyl radical. The induction period in the pyrolysis of ethane. *J.Phys.Chem* **1984,** *88* (23), 5657-5660.
17. Sugawara, K.-I.; Okazaki, K.; Sato, S. Temperature dependence of the rate constants of H and D-atom additions to C_2H_4, C_2H_3D, C_2D_4, C_2H_2, and C_2D_2. *Bulletin of the Chemical Society of Japan* **1981,** *54* (10), 2872-2877.
18. Yang, X.; Tranter, R. S. High-temperature dissociation of ethyl radicals and ethyl iodide. *Int. J. Chem. Kinet.* **2012,** *44* (7), 433-443.
19. Matsugi, A., Roaming Dissociation of Ethyl Radicals. *J.Phys.Chem.Lett* **2013,** *4* (24), 4237-4240.
20. Gilbert, T.; Grebner, T. L.; Fischer, I.; Chen, P. Microcanonical rates for the unimolecular dissociation of the ethyl radical. *J.Chem.Phys* **1999,** *110* (12), 5485-5488.

21. Steinbauer, M.; Giegerich, J.; Fischer, K. H.; Fischer, I. The photodissociation dynamics of the ethyl radical, C_2H_5, investigated by velocity map imaging. *J.Chem.Phys* **2012,** *137* (1), 014303.
22. Seakins, P.; Robertson, S.; Pilling, M.; Slagle, I.; Gmurczyk, G.; Bencsura, A.; Gutman, D.; Tsang, W. Kinetics of the unimolecular decomposition of isopropyl: weak collision effects in helium, argon, and nitrogen. *J.Phys.Chem* **1993,** *97* (17), 4450-4458.
23. Kerr, J. A.; Parsonage, M. J. Evaluated kinetic data on gas phase addition reactions. Reactions of atoms and radicals with alkenes, alkynes and aromatic compounds. 1972.
24. Munk, J.; Pagsberg, P.; Ratajczak, E.; Sillesen, A. Spectrokinetic studies of i-C_3H_7 and i-$C_3H_7O_2$ radicals. *Chem. Phys. Lett* **1986,** *132* (4-5), 417-421.
25. Kurylo, M. J.; Peterson, N. C.; Braun, W. Temperature and pressure effects in the addition of H atoms to propylene. *J.Chem.Phys* **1971,** *54* (11), 4662-4666.
26. Watanabe, T.; Kyogoku, T.; Tsunashima, S.; Sato, S.; Nagase, S. Kinetic isotope effects in the H+ C_3H_6→ C_3H_7 reaction. *Bulletin of the Chemical Society of Japan* **1982,** *55* (12), 3720-3723.
27. Rosado-Reyes, C. M.; Manion, J. A.; Tsang, W. H atom attack on propene. *J.Phys.Chem.A* **2011,** *115* (13), 2727-2734.
28. Hidaka, Y.; Nakamura, T.; Tanaka, H.; Jinno, A.; Kawano, H.; Higashihara, T. Shock tube and modeling study of propene pyrolysis. *Int. J. Chem. Kinet.* **1992,** *24* (9), 761-780.
29. Löser, U.; Scherzer, K.; Weber, K. Abschätzung kinetischer Daten für H-Transferreaktionen mit Hilfe der „Bond Strength-Bond Length (BSBL)"-Methode. *Zeitschrift für Physikalische Chemie* **1989,** *270* (1), 237-245.
30. Harris, G.; Pitts Jr, J. Absolute rate constants and temperature dependencies for the gas phase reactions of H atoms with propene and the butenes in the temperature range 298 to 445 K. *J.Chem.Phys* **1982,** *77* (8), 3994-3997.
31. Nagaraja, S. S.; Liang, J.; Dong, S.; Panigrahy, S.; Sahu, A.; Kukkadapu, G.; Wagnon, S. W.; Pitz, W. J.; Curran, H. J. A hierarchical single-pulse shock tube pyrolysis study of C_2–C_6 1-alkenes. *Combust. Flame* **2020,** *219*, 456-466.
32. Wang, Q.-D.; Liu, Z.-W. Reaction Kinetics of Hydrogen Atom Abstraction from C_4–C_6 Alkenes by the Hydrogen Atom and Methyl Radical. *J.Phys.Chem.A* **2018,** *122* (23), 5202-5210.
33. Nagaraja, S. S.; Kukkadapu, G.; Panigrahy, S.; Liang, J.; Lu, H.; Pitz, W. J.; Curran, H. J. A pyrolysis study of allylic hydrocarbon fuels. *Int. J. Chem. Kinet.* **2020,** *52* (12), 964-978.
34. Tsang, W. Chemical kinetic data base for hydrocarbon pyrolysis. *Industrial & engineering chemistry research* **1992,** *31* (1), 3-8.
35. Tsang, W. Chemical kinetic data base for combustion chemistry part V. Propene. *J.Phys.Chem.Ref.Data* **1991,** *20* (2), 221-273.
36. Frisch, M. J.; Trucks, G. W.; Schlegel, H. B.; Scuseria, G. E.; Robb, M. A.; Cheeseman, J. R.; Scalmani, G.; Barone, V.; Petersson, G. A.; Nakatsuji, H.; t al. *Gaussian 09*, Gaussian 09, revision D.01; 2009.
37. Frisch, M. J.; Trucks, G. W.; Schlegel, H. B.; Scuseria, G. E.; Robb, M. A.; Cheeseman, J. R.; Scalmani, G.; Barone, V.; Petersson, G. A.; Nakatsuji, H.; et al. *Gaussian 16 Rev. B.01*, Wallingford, CT, 2016.
38. Chai, J.-D.; Head-Gordon, M. Long-range corrected hybrid density functionals with damped atom-atom dispersion corrections. *Phys. Chem. Chem. Phys.* **2008,** *10* (44), 6615-6620.
39. Dunning, T. H. Gaussian-basis sets for use in correlated molecular calculations .1. The atoms boron through neon and hydrogen. *J. Chem. Phys.* **1989,** *90* (2), 1007-1023.
40. Georgievskii, Y.; Miller, J. A.; Burke, M. P.; Klippenstein, S. J. Reformulation and solution of the master equation for multiple-well chemical reactions. *J. Phys. Chem. A* **2013,** *117* (46), 12146-12154.
41. Goldsmith, C. F.; Magoon, G. R.; Green, W. H. Database of small molecule thermochemistry for combustion. *J. Phys. Chem. A* **2012,** *116* (36), 9033-9057.
42. Miller, J. A.; Klippenstein, S. J. The recombination of propargyl radicals and other reactions on a C_6H_6 potential. *J.Phys.Chem.A* **2003,** *107* (39), 7783-7799.

43. Simmie, J. M.; Black, G.; Curran, H. J.; Hinde, J. P. Enthalpies of formation and bond dissociation energies of lower alkyl hydroperoxides and related hydroperoxy and alkoxy radicals. *J. Phys. Chem. A* **2008,** *112* (22), 5010-5016.
44. McBride, B. J.; Gordon, S. Computer program for calculating and fitting thermodynamic functions, 1992.
45. Johnston, H. S.; Heicklen, J. Tunnelling corrections for unsymmetrical Eckart potential energy barriers. *J. Phys. Chem.* **1962,** *66* (3), 532-533.
46. Li, Y.; Klippenstein, S. J.; Zhou, C.-W.; Curran, H. J. Theoretical kinetics analysis for Ḣ atom addition to 1,3-butadiene and related reactions on the $\dot{C}_4H_7$ potential energy surface. *J.Phys.Chem.A* **2017,** *121* (40), 7433-7445.
47. Miyoshi, A. Computational studies on the reactions of 3-butenyl and 3-butenylperoxy radicals. *Int. J. Chem. Kinet.* **2010,** *42* (5), 273-288.
48. Klippenstein, S. J.; Miller, J. A. The addition of hydrogen atoms to diacetylene and the heats of formation of i-C_4H_3 and n-C_4H_3. *J.Phys.Chem.A* **2005,** *109* (19), 4285-4295.
49. Klippenstein, S. J.; Miller, J. A.; Jasper, A. W. Kinetics of propargyl radical dissociation. *J.Phys.Chem.A* **2015,** *119* (28), 7780-7791.
50. Ruscic, B.; Pinzon, R. E.; Laszewski, G. v.; Kodeboyina, D.; Burcat, A.; Leahy, D.; Montoy, D.; Wagner, A. F. Active thermochemical tables: thermochemistry for the 21st century. *J. Phys.* **2005,** *16*, 561-570.
51. Ruscic, B.; Pinzon, R. E.; Morton, M. L.; von Laszevski, G.; Bittner, S. J.; Nijsure, S. G.; Amin, K. A.; Minkoff, M.; Wagner, A. F. Introduction to active thermochemical tables: several "key" enthalpies of formation revisited. *J. Phys. Chem. A* **2004,** *108* (45), 9979-9997.
52. Klippenstein, S. J.; Harding, L. B.; Ruscic, B. Ab initio computations and active thermochemical tables hand in hand: heats of formation of core combustion species. *J. Phys. Chem. A* **2017,** *121* (35), 6580-6602.
53. Simmie, J. M.; Somers, K. P. Benchmarking compound methods (CBS-QB3, CBS-APNO, G3, G4, W1BD) against the active thermochemical tables: a litmus test for cost-effective molecular formation enthalpies. *J. Phys. Chem. A* **2015,** *119* (28), 7235-7246.
54. Somers, K. P.; Simmie, J. M., Benchmarking compound methods (CBS-QB3, CBS-APNO, G3, G4, W1BD) against the active thermochemical tables: formation enthalpies of radicals. *J. Phys. Chem. A* **2015,** *119* (33), 8922-8933.
55. Simmie, J. M.; Somers, K. P.; Metcalfe, W. K.; Curran, H. J. Substituent effects in the thermochemistry of furans: A theoretical (CBS-QB3, CBS-APNO and G3) study. *J. Chem. Thermodyn.* **2013,** *58*, 117-128.
56. Burcat, A.; Ruscic, B. Third millenium ideal gas and condensed phase thermochemical database for combustion (with update from active thermochemical tables); Argonne National Lab.(ANL), Argonne, IL (United States): 2005.
57. Curran, H. J. Rate constant estimation for C_1 to C_4 alkyl and alkoxyl radical decomposition. *Int. J. Chem. Kinet.* **2006,** *38* (4), 250-275.
58. Kyogoku, T.; Watanabe, T.; Tsunashima, S.; Sato, S. Arrhenius parameters for the reactions of hydrogen and deuterium atoms with four butenes. *Bulletin of the Chemical Society of Japan* **1983,** *56* (1), 19-21.
59. Awan, I. A.; Burgess, D. R., Jr.; Manion, J. A. Pressure dependence and branching ratios in the decomposition of 1-pentyl radicals: shock tube experiments and master equation modeling. *J. Phys Chem. A* **2012,** *116* (11), 2895-910.
60. Comandini, A.; Awan, I. A.; Manion, J. A. Thermal decomposition of 1-pentyl radicals at high pressures and temperatures. *Chem. Phys. Lett.* **2012,** *552*, 20-26.
61. Jitariu, L. C.; Jones, L. D.; Robertson, S. H.; Pilling, M. J.; Hillier, I. H. Thermal rate coefficients via variational transition state theory for the unimolecular decomposition/isomerization of 1-pentyl radical: ab initio and direct dynamics calculations. *J. Phys. Chem. A* **2003,** *107* (41), 8607-8617.

62. Jasper, A. W.; Hansen, N. Hydrogen-assisted isomerizations of fulvene to benzene and of larger cyclic aromatic hydrocarbons. *Proc. Combust Inst.* **2013,** *34* (1), 279-287.

TOC image.